STRUCTURAL CONTROL AND HEALTH MONITORING
Struct. Control Health Monit. 2009; **16**:800–841
Published online 28 August 2009 in Wiley InterScience
(www.interscience.wiley.com). DOI: 10.1002/stc.349

Adaptive passive, semiactive, smart tuned mass dampers: identification and control using empirical mode decomposition, hilbert transform, and short-term fourier transform

S. Nagarajaiah*,†

Department of Civil and Environmental Engineering and Department of Mechanical Engineering and Material Science, Rice University, Houston, TX 77005, U.S.A.

SUMMARY

Tuned mass dampers (TMD), active mass dampers (AMD) and hybrid mass dampers (HMD) have been widely applied for vibration control of tall buildings and bridges in the past decade. Recently, the author and his coworkers have developed semiactive or smart tuned mass dampers (STMD) using semiactive variable stiffness systems. STMD's are superior than TMD's in reducing the response of the primary structure. In case the fundamental frequency of the primary structure changes due to damage or deterioration, then the TMD will be off-tune; hence, it will lose its effectiveness significantly, whereas the STMD is robust against such changes as it is always tuned. The author and his coworkers have shown that STMD can provide performance similar to AMD/HMD, but with an order of magnitude less power consumption.

In this paper, new adaptive length pendulum STMD's are introduced. The concept of adaptive passive tuned mass dampers (APTMD) is introduced. APTMD is a TMD in which a tuning parameter such as frequency is adjusted passively based on some local mechanical feedback (displacement, velocity, rotation, etc.), but without associated sensing and computer feedback needed in a STMD. Also, the concept of STMD is further developed in this paper and practical STMD's and APTMD's implementation in USA, Japan, and China is presented.

Systems with semiactive variable stiffness devices and STMD/APTMD are linear time varying systems (LTV); hence, algorithms are needed for their identification and control. Recently, the author and his coworkers have developed instantaneous frequency tracking control algorithms. In this paper new system identification algorithms based on time frequency methods, such as Empirical Mode Decomposition (EMD), Hilbert Transform (HT), and short time Fourier transform (STFT), are developed. New real time tuning algorithms that identify the instantaneous frequency of the LTV system and tune the STMD are developed based on EMD, HT, and STFT. Systems with STMD subjected to stationary (harmonic,

*Correspondence to: S. Nagarajaiah, CEVE and MEMS, MS318, Rice University, 6100 Main Street, Houston, TX 77005, U.S.A.
†E-mail: nagaraja@rice.edu, satish.nagarajaiah@rice.edu

Contract/grant sponsor: National Science Foundation; contract/grant numbers: NSF-CMMI 0830391, NSF-CMS-9996290

Received 30 June 2008
Revised 2 June 2009
Accepted 10 June 2009

sinsweep, and white-noise) and nonstationary (earthquake) excitations are investigated. The effectiveness of the STMD systems and the new identification and control algorithms is demonstrated by means of numerical simulations and experimental validation. Copyright © 2009 John Wiley & Sons, Ltd.

KEY WORDS: semiactive; smart tuned mass dampers; adaptive passive tuned mass dampers; tuned vibration absorbers; dynamic vibration absorbers; system identification; control; dynamic response; time-frequency methods; empirical mode decomposition; Hilbert-transform; short time Fourier transform

1. INTRODUCTION

Professor Takuji Kobori was a pioneer in developing and implementing structural control technology [1]. His contributions are numerous: but, his favorite invention was variable stiffness system [2], which he pioneered. Kobori *et al*. [3] developed worlds first active variable stiffness system (AVS). In the AVS system the building stiffness is altered based on the nature of the earthquake, which results in the non-resonant state. The AVS system has been implemented in a full-scale structure in Tokyo, Japan [3]. The observed response of the structure with the AVS system in two earthquakes in Tokyo indicated the potential of such devices; however, abrupt switching in the AVS system was a limiting factor as observed in one of the earthquakes [4]. The AVS system was one of the first variable stiffness systems implemented in civil engineering structures. Another first for active structural control was the implementation of active tuned mass dampers (ATMD) [5] in a medium rise building in 1989 by Professor Kobori and his coworkers at Kajima [6]. Then came the implementation of active tendon system and ATMD by researchers at SUNY Buffalo [7].

Semi-active control of linear and nonlinear structures using innovative devices such as variable damping systems [8] and variable stiffness systems has gained considerable attention in the recent years [9]. Practical implementation issues of such systems have been addressed by Chu *et al*. [10]. In such systems variation in stiffness or damping of the system is used to control the response as compared to direct application of control force in fully active systems; hence, these systems need nominal power. Reliability of the semi-actively controlled systems is an added advantage, as these can operate as a passive device in extreme cases. Researchers have developed variable stiffness devices, which are similar in nature to AVS [11,12], but are based on pneumatic systems, instead of hydraulic systems of AVS. A new semi-active continuously and independently variable stiffness (SAIVS) device has been developed by the author [13] to overcome limitations of existing systems. This device can switch the stiffness continuously and smoothly. Analytical and experimental studies on SAIVS device indicate the potential of the device in reducing the response [14].

1.1. Smart tuned mass dampers

The Tuned Mass Damper (TMD) is a passive energy-absorbing system [15,16] consisting of a secondary mass, a spring, and a viscous damper attached to a primary system to reduce undesirable vibrations. The TMD has many advantages compared with other damping devices: reliability, efficiency, and low maintenance cost amongst others. Hence in recent years it has been widely used in civil engineering structures [17,18]. Many researchers have studied the

DOI: 10.1002/stc

advantages and effectiveness of TMD and have proposed various schemes to improve their robustness and reliability. Tuned liquid dampers have also been developed [19].

Most often, in a structure, the first vibrational frequency and mode of the primary system plays a dominant role in the dynamic response. To be effective TMD must remain tuned to the first mode frequency of the original primary system [15,16]. However, as it is well known, the TMD is very sensitive to even a small change in the tuning, which can be a disadvantage.

The use of more than one TMD i.e. multiple TMD (MTMD) [20–25] with different dynamic characteristics to improve the robustness has been proposed. However, like a single TMD, MTMD's are not robust under variations in both the primary structures natural frequencies and the damping ratio. The use of an active TMD provides one possibility to overcome these drawbacks [5,6]. ATMD and active mass dampers (AMD) have also been developed and implemented widely for applications in response control [5,6,9] of buildings and bridges. Active TMD can be more robust to tuning error with the appropriate use of feedback and can be effective in reducing response, but with associated need for application of active forces and substantial power requirement to operate. Semi-active control of STMD [26–33] and STLD [34] offer an attractive alternative to provide a comparable performance with an order of magnitude less power requirement [31,35].

The smart tuned mass damper (STMD) and smart multiple tuned mass damper, developed by the author and his coworkers [31,32,36], is capable of continuously varying its stiffness and retuning its frequency due to real time control, and is robust to changes in building stiffness and damping. In comparison, the passive TMD can only be tuned to the first mode frequency of the building. The building fundamental frequency can change due to damage or other reasons. The developed STMD overcomes the limitations of the TMD (i.e. detuning) by retuning the frequency in real time. The device requires an order of magnitude less power [31,35].

1.2. Note on tuning of STMD

STMD can be tuned to the first mode of the primary system or the dominant response frequency (close to a selected mode–usually the first mode), at which the primary system is responding [31,36,37], or can be tuned to the dominant excitation frequency [32]. In this paper we tune to the dominant frequency, at which the primary system is responding, by tracking it using the top floor displacement response of the building.

Another important aspect is the tuning of the instantaneous frequency of STMD using either variable stiffness or variable damping. It is more efficient to use variable stiffness to effect the change in instantaneous frequency rather than variable damping, although it is possible to develop STMD with variable damping [29]. Researchers who develop such systems seldom 'retune' frequency of TMD, they focus more on energy dissipation by using linear quadratic controllers or similar techniques [29]. The relationship between damped natural frequency of a TMD, ω_d, and its undamped natural frequency ω_n, and damping ratio, ξ, is $\omega_d = \omega_n\sqrt{1-\xi^2}$. The easiest way to change the ω_d of a TMD is by changing its stiffness (since mass remains constant) or 'tuning' ω_n. Alternatively, the damping ratio ξ can be changed; but to affect even small changes of ω_d, ξ needs to change substantially, which defeats the purpose of TMD, as tuning no longer dominates, but damping does. Additionally, in Section 6 it will be shown that increasing damping beyond the optimal is not beneficial. Would it be judicious to adjust damping in light of the requirement of optimal damping and tuning as well? It certainly seems more desirable to tune using stiffness rather than damping, unless there are other compelling reasons such as stroke limitations.

DOI: 10.1002/stc

1.3. Adaptive length pendulum TMD and adaptive passive TMD

In this paper, new adaptive length pendulum (ALP) STMD's are introduced. The concept of adaptive passive tuned mass dampers (APTMD) is introduced. APTMD is a TMD in which a tuning parameter such as frequency is adjusted passively based on some local mechanical feedback (displacement, velocity, rotation, etc.), but without associated sensing and computer feedback needed in a STMD. Also, the concept of STMD is further developed in this paper and practical STMD's and APTMD's implementation in USA, Japan, and China are presented.

Systems with semiactive variable stiffness devices and STMD/APTMD are linear time varying systems (LTV); hence, algorithms are needed for their identification and control. Recently, the author and his coworkers have developed instantaneous frequency tracking control algorithms. In this paper new system identification algorithms based on time frequency methods, such as Empirical Mode Decomposition (EMD), Hilbert Transform (HT) and short time Fourier transform (STFT), are developed. New real time tuning algorithms that identify the instantaneous frequency of the LTV system and tune the STMD are developed based on EMD, HT, and STFT. Systems with STMD subjected to stationary (harmonic, sinsweep, and white-noise) and non-stationary (earthquake) excitations are investigated. The effectiveness of the STMD systems and the new identification and control algorithms is demonstrated by means of numerical simulations and experimental validation.

The outline of the paper is as follows: Section 2 presents time frequency techniques, such as HT, STFT, EMD; Section 3 presents new system identification using EMD/HT; Section 4 presents the SAIVS device; Section 5 presents the mathematical formulation of LTV with STMD; Section 6 presents the new real time tuning control algorithms for tuning STMD and the numerical results; Section 7 presents a new ALP STMD and its experimental validation; Section 8 presents practical STMD and APTMD concepts and their implementation; and Section 9 presents the conclusions.

2. TIME-FREQUENCY TECHNIQUES: HT, STFT, AND EMD

2.1. Analytical signal and HT

Signals in nature are real valued but for analysis it is often more convenient to deal with complex signals. One wants the real part, $s(t)$, of the complex signal, $s_a(t)$, to be the actual signal under consideration. How does one fix the imaginary part, $\bar{s}(t)$, to form the complex signal? In particular if one wants to write a complex signal, how does one choose $\bar{s}(t)$? The standard method is to form the 'analytic' signal, $s_a(t)$,

$$s_a(t) = s(t) + \mathrm{j}\bar{s}(t) \tag{1}$$

where $\mathrm{j} = \sqrt{-1}$.

This can be achieved by taking the spectrum of the actual signal, $s(\omega)$, deleting the negative part of the spectrum, retaining only the positive part of the spectrum, multiply it by a factor of 2, and then form the new (complex) signal by Fourier inversion. More specifically if one has a real signal, $s(t)$, calculate $s(\omega)$. Form the complex signal with the positive part of $s(\omega)$ only,

$$s_a(t) = 2\frac{1}{\sqrt{2\pi}}\int_0^\infty s(\omega)\mathrm{e}^{\mathrm{j}\omega t}\,\mathrm{d}\omega \tag{2}$$

DOI: 10.1002/stc

The factor of two is inserted so that the real part of the complex signal will be equal to the real signal one started out with. Therefore substituting for $s(\omega)$

$$s_a(t) = \frac{1}{\pi}\int_0^\infty \int s(t')\mathrm{e}^{-\mathrm{j}\omega t'}\mathrm{e}^{\mathrm{j}\omega t}\,\mathrm{d}t'\,\mathrm{d}\omega \tag{3}$$

Using the fact that

$$\int_0^\infty \mathrm{e}^{\mathrm{j}\omega x}\,\mathrm{d}\omega = \pi\delta(x) + \frac{\mathrm{j}}{x} \tag{4}$$

One has

$$\int_0^\infty \mathrm{e}^{\mathrm{j}\omega(t-t')}\mathrm{d}\omega = \pi\delta(t-t') + \frac{\mathrm{j}}{t-t'} \tag{5}$$

Hence

$$s_a(t) = \frac{1}{\pi}\int s(t')\left(\pi\delta(t-t') + \frac{\mathrm{j}}{t-t'}\right)\mathrm{d}t' \tag{6}$$

Or

$$s_a(t) = s(t) + \frac{\mathrm{j}}{\pi}\int_{-\infty}^\infty \frac{s(t')}{t-t'}\,\mathrm{d}t' \tag{7}$$

The imaginary part turns out to be the HT:

$$\bar{s} = H[s(t)] = \frac{1}{\pi}\int_{-\infty}^\infty \frac{s(t')}{t-t'}\,\mathrm{d}t' \tag{8}$$

Hence,

$$s_a(t) = s(t) + \mathrm{j}H[s(t)] = s(t) + \mathrm{j}\bar{s} \tag{9}$$

The complex signal thus formed, $s_a(t)$, is called the analytic signal. Note that by definition analytic signals are signals whose spectrum consists only of positive frequencies. That is, the spectrum is zero for negative frequencies.

As per Equations (1)–(9), the analytic signal can be obtained by: (1) taking the Fourier transform of $s(t)$; (2) zeroing the amplitude for negative frequencies and doubling the amplitude for positive frequencies; and (3) taking the inverse Fourier transform. The analytic signal $s_a(t)$ can also be expressed as

$$s_a(t) = A(t)\mathrm{e}^{\mathrm{j}\varphi(t)} \tag{10}$$

where $A(t) =$ instantaneous amplitude and $\varphi(t) =$ instantaneous phase.

2.2. Instantaneous frequency

In the analytic signal given by Equations (1) and (10), $A(t) = \sqrt{(s^2(t) + \bar{s}^2(t)}$ and $\varphi(t) = \arctan\left(\frac{\bar{s}(t)}{s(t)}\right)$, the instantaneous frequency $\omega_i(t)$ is given by

$$\omega_i(t) = \dot{\varphi}(t) = \frac{\mathrm{d}}{\mathrm{d}t}\left(\arctan\left(\frac{\bar{s}(t)}{s(t)}\right)\right) \tag{11}$$

DOI: 10.1002/stc

where

$$\frac{\mathrm{d}\varphi}{\mathrm{d}t} = \frac{1}{1 + \left(\dfrac{\bar{s}^2(t)}{s^2(t)}\right)^2} \frac{\mathrm{d}\dfrac{\bar{s}(t)}{s(t)}}{\mathrm{d}t} \tag{12}$$

and

$$\frac{\mathrm{d}}{\mathrm{d}t}\frac{\bar{s}(t)}{s(t)} = \frac{s(t)\dot{\bar{s}}(t) - \bar{s}(t)\dot{s}(t)}{s^2(t)} \tag{13}$$

From Equations (12) and (13) one gets

$$\omega_i(t) = \frac{\mathrm{d}\varphi(t)}{\mathrm{d}t} = \frac{(s(t)\dot{\bar{s}}(t) - \bar{s}(t)\dot{s}(t))}{s^2(t) + \bar{s}^2(t)} \tag{14}$$

2.3. Short-time Fourier transform and spectrogram

The Fourier transform (FT) of a signal $s(t)$ is given by $s(\omega) = \dfrac{1}{\sqrt{2\pi}} s(t)\mathrm{e}^{-\mathrm{j}\omega t}\, dt$. The short-time Fourier transform (STFT), the first tool devised for analyzing a signal in both time and frequency, is based on FT of a short portion of signal $s_h(\tau)$ sampled by a moving window $h(\tau - t)$. The running time is τ and the fixed time is t. Since time interval is short compared to the whole signal this process is called taking the STFT.

$$S_t(\omega) = \frac{1}{\sqrt{2\pi}} \int_{-\infty}^{\infty} s_h(\tau)\mathrm{e}^{-\mathrm{j}\omega\tau}\, \mathrm{d}\tau \tag{15}$$

where $s_h(\tau)$ is defined as follows:

$$s_h(\tau) = s(\tau)h(\tau - t) \tag{16}$$

in which $h(\tau - t)$ is an appropriately chosen window function that emphasizes the signal around the time t, and is a function $\tau - t$ i.e. $s_h(\tau) = s(\tau)$ for τ near t and $s_h(\tau) = 0$ for τ far away from t. Considering this signal as a function of τ one can ask for the spectrum of it. Since the window has been chosen to emphasize signal at t the spectrum will emphasize the frequencies at that time and hence give an indication of the frequencies at that time. In particular the spectrum is,

$$S_t(\omega) = \frac{1}{\sqrt{2\pi}} \int_{-\infty}^{\infty} s(\tau)h(\tau - t)\mathrm{e}^{-\mathrm{j}\omega\tau}\, \mathrm{d}\tau \tag{17}$$

which is the STFT.

Summarizing, the basic idea is that if one wants to know the frequency content of the signal at a particular time, t, then take a small piece $s_h(\tau)$ of the signal around that time and Fourier analyze it, neglecting the rest of the signal, obtaining a spectrum at that time. Next take another small piece, of equal length of the signal, at the next time instant and get another spectrum. Keep marching forward till the entire signal is sampled. The collection of all these spectrum (or slices at every time instant) gives a time-frequency spectrogram, which covers the entire signal, and captures the localized time varying frequency content of the signal. If one performs a FT then the localized variations of frequency content are lost, since FT is performed on the whole signal; one gets an average spectrum of all those obtained by STFT.

DOI: 10.1002/stc

The energy density of the modified signal and the spectrogram is given by,

$$P(t,\omega) = |S_t(\omega)|^2 \tag{18a}$$

or

$$P_{SP}(t,\omega) = \left| \frac{1}{\sqrt{2\pi}} \int_{-\infty}^{\infty} s(\tau) h(\tau - t) \mathrm{e}^{-\mathrm{j}\omega\tau} \, \mathrm{d}\tau \right|^2 \tag{18b}$$

By analogy with the previous discussion it can be used to study the behavior of the signal around the frequency point ω. This is done by choosing a window function whose transform is weighed relatively higher at the frequency ω.

$$H(\omega) = \frac{1}{\sqrt{2\pi}} \int_{-\infty}^{\infty} h(t) \mathrm{e}^{-\mathrm{j}\omega t} \, \mathrm{d}t \tag{19a}$$

$$s_\omega(t) = \frac{1}{\sqrt{2\pi}} \int_{-\infty}^{\infty} S(\omega') H(\omega - \omega') \mathrm{e}^{\mathrm{j}\omega' t} \, \mathrm{d}\omega' \tag{19b}$$

$$s_h(\tau) = s(\tau) h(\tau - t) = \frac{1}{\sqrt{2\pi}} \int_{-\infty}^{\infty} S_t(\omega) \mathrm{e}^{\mathrm{j}\omega t} \, \mathrm{d}\omega \tag{19c}$$

where ω' is running frequency and fixed frequency is ω. The spectrogram is given by

$$P_{SP}(t,\omega) = \left| \frac{1}{\sqrt{2\pi}} \int_{-\infty}^{\infty} s(\omega') H(\omega - \omega') \mathrm{e}^{\mathrm{j}\omega' t} \, \mathrm{d}\omega' \right|^2 \tag{20}$$

The limitation of STFT is its fixed resolution, which can be overcome multiresolution analysis using wavelets [38,39]. In STFT the length of the signal segment chosen or the length of the windowing function $h(t)$ determines the resolution: broad window results in better frequency resolution but poor time resolution, and narrow window results in good time resolution but poor frequency resolution, due to the time-bandwidth relation (uncertainty principle [40]). Note $h(t)$ and $H(\omega)$ are Fourier transform pairs (Equation (19a)), i.e. if $h(t)$ is narrow, more time resolution is obtained; however, $H(\omega)$ becomes broad resulting in poor frequency resolution and vice versa.

2.4. STFT implementation procedure

The implementation procedure for the STFT in the discrete domain is carried out by extracting time windows of the original nonstationary signal $s(t)$. After zero padding and convolving the signal with Hamming window, the DFT is computed for each windowed signal to obtain STFT, $S_t(\omega)$, of signal $s_h(\tau)$. If the window width is $n.\Delta t$ (where n is number of points in the window, and Δt is the sampling rate of the signal), the k-th element in $S_t(\omega)$ is the Fourier coefficient that corresponds to the frequency,

$$\omega_k = \frac{2\pi k}{n.\Delta t} \text{ (for window width } n.\Delta t) \tag{21}$$

To illustrate the STFT method is applied to the acceleration time history of the 1994 Northridge Sylmar earthquake (fault parallel component 90°) as an example. Figure 1 shows the time history (upper left), frequency spectrum (lower right), the time-frequency distribution of the spectrogram (upper right), and spectrogram (lower left) of the Sylmar earthquake

DOI: 10.1002/stc

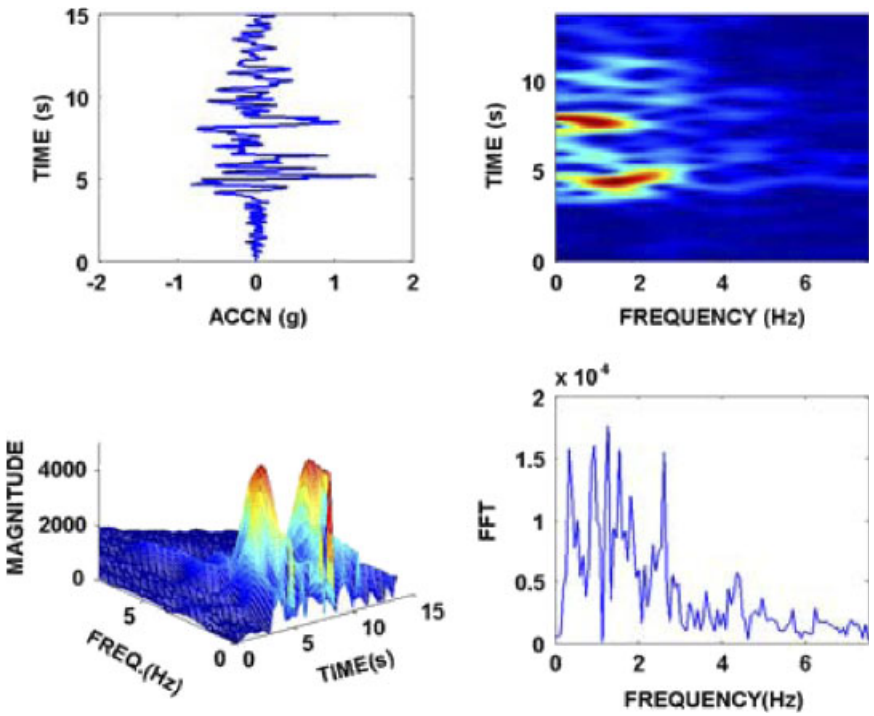

Figure 1. Time–frequency analysis of Sylmar earthquake.

acceleration signal. The evolution of the frequency content of the Sylmar signal as a function of time can be seen in the spectrogram shown in Figure 1 (lower left), and from time-frequency distribution (upper right). If one examines the time history alone (upper left) or the frequency spectrum (lower right) alone, the localized nature of the time varying frequency content is not evident.

2.5. Empirical mode decomposition

For a multicomponent signal—as in a multimodal or multidegree of freedom (MDOF) response—the procedure described in the previous section to obtain analytic signal and instantaneous frequency cannot be applied directly, as it is meant for monocomponent signals. The EMD technique, developed by Huang [41], adaptively decomposes a signal into 'intrinsic mode functions' (IMF), which can then be converted to analytical signal using HT. The time-frequency representation and instantaneous frequency can be obtained from the intrinsic modes extracted from the decomposition, using HT. The principle technique is to decompose a signal into a sum of functions that (1) have the same numbers of zero crossings and extrema, and (2) are symmetric with respect to the local mean. The first condition is similar to the narrow-band requirement for a stationary Gaussian process. The second condition modifies a global requirement to a local one, and is necessary to ensure that the instantaneous frequency will not have unwanted fluctuations as induced by asymmetric waveforms. These functions are called IMF (denoted by imf_i) obtained iteratively (Huang *et al.* 1998 [41]). The

DOI: 10.1002/stc

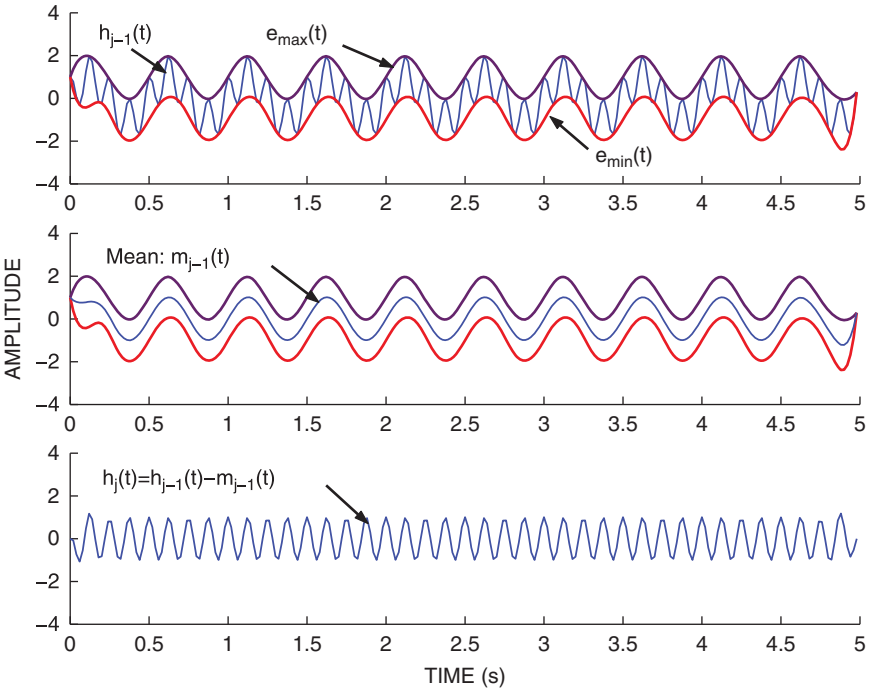

Figure 2. EMD of double harmonic signal.

signal, $x_j(t)$, for example, jth degree of freedom displacement of a MDOF system, can be decomposed as follows

$$x_j(t) = \sum_{i=1}^{n} \text{imf}_i(t) + r_n(t) \tag{22}$$

where $\text{imf}_i(t)$ are the 'IMF' (note: dominant IMFs are equivalent to individual modal contributions to $x_j(t)$, which will be demonstrated in a later section) and $r_n(t)$ is the residue of the decomposition. The IMF are obtained using the following algorithm (Figure 2):

1. Initialize; $r_0 = x_j(t), i = 1$
2. Extract the imf_i as follows:
   (a) Initialize: $h_0(t) = r_{i-1}(t), j = 1$
   (b) Extract the local minima and maxima of $h_{j-1}(t)$
   (c) Interpolate the local maxima and the local minima by a spline to form upper and lower envelopes of $h_{j-1}(t)$, $e_{\max}(t)$ and $e_{\min}(t)$ respectively.
   (d) Calculate the mean m_{j-1} of the upper and lower envelopes $= (e_{\max}(t) + e_{\min}(t))/2$
   (e) $h_j(t) = h_{j-1}(t) - m_{j-1}(t)$
   (f) If stopping criterion is satisfied then set $\text{imf}_i(t) = h_j(t)$ else go to (b) with $j = j + 1$
3. $r_i(t) = r_{i-1}(t) - \text{imf}_i(t)$
4. If $r_i(t)$ still has at least 2 extrema then go to 2 with $i = i + 1$ else the decomposition is finished and $r_i(t)$ is the residue.

DOI: 10.1002/stc

The analytical signal, $s_a(t)$, and the instantaneous frequencies $\omega_i(t)$, associated with each $\text{imf}_i(t)$ component, can be obtained using Equations (1)–(14) by letting $s(t) = \text{imf}_i(t)$ and $s_a(t) = s(t) + \text{j}H(s(t))$ for each IMF component.

To ensure that the IMF components retain the amplitude and frequency modulations of the actual signal, a satisfactory stopping criteria for the sifting process are defined [42]. A criteria for stopping are accomplished by limiting the standard deviation, SD [41], of $h(t)$, obtained from consecutive sifting results as

$$\text{SD} = \sum_{k=0}^{l} \left[\frac{|(h_{j-1}(k\Delta t) - h_j(k\Delta t))|^2}{h_{j-1}^2(k\Delta t)} \right] \tag{23}$$

where $l = T/\Delta t$ and $T =$ total time. A typical value for SD is set between 0.2 and 0.3 [42]. An improvement over this criterion is based on two thresholds θ_1 and θ_2, aimed at globally small fluctuations in the mean while taking into account locally large excursions. This amounts to introducing a mode amplitude $a(t)$ and an evaluation function $\sigma(t)$:

$$a(t) = \left(\frac{e_{\max}(t) - e_{\min}(t)}{2} \right) \tag{24}$$

$$\sigma(t) = \left| \frac{m(t)}{a(t)} \right| \tag{25}$$

Sifting is iterated until $\sigma(t) < \theta_1$ for a fraction of the total duration while $\sigma(t) < \theta_2$ for the remaining fraction. Typically $\theta_1 \approx 0.05$ and $\theta_2 \approx 10\theta_1$ [42].

3. SYSTEM IDENTIFICATION USING EMD/HT

EMD can be used to decompose a signal into its multimodal components (+ residual IMF components + residue). In a lightly damped system with distinct modes, EMD can extract the multicomponent modal contributions [or IMFs] from the jth DOF displacement response of a MDOF system. Each of these IMF components can then be analyzed separately to obtain the instantaneous frequency and damping ratios. If the displacement of MDOF system is represented by vector $\mathbf{x} = \Phi\mathbf{q}$, where $\Phi =$ modal matrix, $\mathbf{q}$ = modal displacement vector, then combining it with Equation (22) leads to the following equation for $x_j(t)$, the jth degree of freedom displacement of a MDOF system,

$$x_j(t) = \sum_{i=1}^{n} \text{imf}_i(t) + r_n(t) = \sum_{i=1}^{m} \Phi_{ji} q_i(t) + \sum_{i=m}^{n} \text{imf}_i(t) + r_n(t) \tag{26}$$

where m = number of modes of a MDOF system and IMF's from m to n are treated as residual terms along with the actual residual and discarded.

The equation of motion of a MDOF is given by

$$\mathbf{M}\ddot{\mathbf{x}} + \mathbf{C}\dot{\mathbf{x}} + \mathbf{K}\mathbf{x} = \mathbf{M}\mathbf{R}f \tag{27}$$

substituting $\mathbf{x} = \Phi\mathbf{q}$,

$$\mathbf{\Phi}^{\mathbf{T}}\mathbf{M}\mathbf{\Phi}\ddot{\mathbf{q}} + \mathbf{\Phi}^{\mathbf{T}}\mathbf{C}\mathbf{\Phi}\dot{\mathbf{q}} + \mathbf{\Phi}^{\mathbf{T}}\mathbf{K}\mathbf{\Phi}\mathbf{q} = \mathbf{\Phi}^{\mathbf{T}}\mathbf{M}\mathbf{R}f \tag{28}$$

DOI: 10.1002/stc

Proportional damped system with orthonormal Φ leads to m uncoupled equations of motion with

$$\mathrm{diag}[\Lambda_c] = \begin{bmatrix} 2\xi_1\omega_1 & 0 & . & . & . & 0 \\ 0 & 2\xi_2\omega_2 & . & . & . & 0 \\ . & . & . & . & . & . \\ . & . & . & . & . & . \\ . & . & . & . & . & . \\ 0 & 0 & 0 & 0 & 0 & 2\xi_n\omega_n \end{bmatrix}, \quad \mathrm{diag}[\Lambda_k] = \begin{bmatrix} \omega_1^2 & 0 & . & . & . & 0 \\ 0 & \omega_2^2 & . & . & . & 0 \\ . & . & . & . & . & . \\ . & . & . & . & . & . \\ . & . & . & . & . & . \\ 0 & 0 & 0 & 0 & 0 & \omega_n^2 \end{bmatrix}$$

$$\ddot{q}_k + 2\xi_k\omega_k\,\dot{q}_k + \omega_k^2 q_k = \Gamma_k f \tag{29}$$

where $\Gamma_k = \Phi_k^T \mathbf{MR}$. With f as input and q_k as output, taking Laplace transform

$$(s^2 + 2\xi_k\omega_k s + \omega_k^2) q_k(s) = \Gamma_k f(s) \tag{30}$$

Dropping Γ_k for generality, the transfer function is then given by

$$H_k(s) = \frac{1}{s^2 + 2\xi_k\omega_k s + \omega_k^2} \tag{31}$$

and the frequency response function (FRF) is given by

$$H_k(\mathrm{j}\omega) = \frac{1}{-\omega^2 + \mathrm{j}2\xi_k\omega_k\omega + \omega_k^2} \tag{32}$$

Noting $\mathbf{x_k} = \Phi_\mathbf{k} q_k$ and x_{jk} as the jth component of the displacement contributed by the kth mode, and with f as input and x_{jk} as output, the transfer function

$$H_{jk}(\mathrm{j}\omega) = \frac{1}{(\omega_k^2 - \omega^2) + \mathrm{j}2\xi_k\omega_k\omega}\,\phi_{\mathrm{j}k} \tag{33}$$

If the structure is lightly damped, the peak transfer function occurs at $\omega = \omega_k$ with amplitude

$$|H_{jk}(\mathrm{j}\omega)| = \frac{\sqrt{1 + 4\xi_k^2}}{2\xi_k}\,\phi_{jk} \tag{34}$$

From Equation (34) it is seen that magnitudes of the peaks of FRF at $\omega = \omega_k$ are proportional to the components of the kth modal vector. The sign of these components can be determined by phases associated with the FRF's: if two modal components are in phase, they are of the same sign and if the two modal components are out-of-phase, they are of opposite sign. With the knowledge of magnitude of peaks, the damping factor, ξ_k can be solved from Equation (34). From Equation (33) summing over all modes gives

$$H_{ij}(\mathrm{j}\omega) = \sum_{k=1}^{n} \frac{\phi_{ik}\phi_{jk}}{(\omega_k^2 - \omega^2) + \mathrm{j}2\xi_k\omega_k\omega} \tag{35}$$

DOI: 10.1002/stc

which can be written as

$$H_{ij}(\mathrm{j}\omega) = \sum_{k=1}^{n} \frac{{}_kA_{ij}}{(\omega_k^2 - \omega^2) + \mathrm{j}2\xi_k\omega_k\omega} \tag{36}$$

where ${}_kA_{ij} = \phi_{ik}\phi_{jk}$ being the residues or modal components. Taking the inverse transform of Equation (36) gives the general form of the impulse response function (IRF)

$$h_{ij}(t) = \sum_{k=1}^{n} \frac{{}_kA_{ij}}{\omega_{\mathrm{d}k}} \mathrm{e}^{-\xi_k\omega_k t} \sin(\omega_{\mathrm{d}k} t) \tag{37}$$

where $\omega_{dk} = \omega_k\sqrt{1-\xi_k^2}$ = damped frequency of the kth mode. It follows from Equation (36) that MDOF linear time invariant system frequency responses are the sum of n single degree of freedom frequency responses, provided that well separated modes and light proportional damping are valid, and the residues and the modes are real. For non proportional damped systems the residues and modes become complex.

Consider the function $\mathrm{e}^{-\sigma_k+\mathrm{j}\omega_k t}$ with $\sigma_k = \xi_k\omega_{nk}$ and $\omega_k = \omega_{\mathrm{d}k}$, and for a lightly damped asymptotically stable system with ($\xi_k < 10\%$) $\sigma > 0$, we can rewrite the Equation (33) for mode k by taking inverse Fourier transform

$$h_{jk}(t) = A_{jk}\mathrm{e}^{-\sigma_k t} \sin(\omega_{\mathrm{d}k} t) \tag{38a}$$

$$\overline{h}_{jk}(t) = A_{jk}\mathrm{e}^{-\sigma_k t} \cos(\omega_{\mathrm{d}k} t) \tag{38b}$$

where $A_{jk} = \dfrac{\Phi_{jk}}{\omega_{dk}}$ leading to the analytical signal

$$h_{jk_a}(t) = h_{jk}(t) + j\overline{h}_{jk}(t) \tag{39}$$

that can be written as

$$h_{jk_a}(t) = \bar{A}_{jk}\mathrm{e}^{\mathrm{j}\varphi t} \tag{40}$$

The magnitude of this analytical signal is given by

$$|h_{jk_a}(t)| = |\,\overline{A}_{jk}\,| = \sqrt{h_{jk_a}^2(t) + \overline{h}_{jk_a}^2(t)} \tag{41}$$

Substituting Equation (38a) and (38b) and simplifying results in

$$|\,\overline{A}_{jk}\,| = A_{jk}\mathrm{e}^{-\sigma_k t} \tag{42}$$

Taking the natural logarithm of this expression yields

$$\log|\,\overline{A}_{jk}\,| = -\sigma_k t + \log(A_{jk}) = -\xi_k\omega_n t + \log(A_{jk}) \tag{43}$$

The author and coworkers originally developed the EMD/HT system identification approach for tuning STMD in 2001 [37], based on their earlier work [43] on variable stiffness systems. The advantage of this approach is that it is signal based; hence, measured response at any one DOF can be used to make useful estimates of instantaneous frequency and damping ratio. However, to estimate mode shapes response signals at more degrees of freedom will be needed. Each significant IMF component represents one modal component with unique instantaneous frequency and damping ratio.

Individual mode FRF and corresponding IRF can be extracted when band pass filters [44] are applied to the system FRF. Equation (42) can be used to estimate damping in the kth mode, as suggested originally by Thrane [44] in 1984 and adopted by Agneni [45] in 1989. In 2003 Yang and coworkers [46,47] have extended this approach by using EMD/HT to decompose and

DOI: 10.1002/stc

obtain IMFs that are modal responses; they analytically obtained modal-free vibration response and then obtained the instantaneous frequency and damping ratios based on the idea of Thrane [44]. In case when the inputs are white noise excitation (WNE) and the output accelerations at a certain floor are available then they [47] obtain the free vibration response from the stationary response to white noise using the random decrement technique followed by instantaneous frequency and damping calculations. The procedure outlined below was developed independently by the author and coworkers [37].

The EMD/HT system identification procedure [37] is as follows:

1. Obtain signal $x_j(t)$, jth degree of freedom displacement of a MDOF system, from the feedback response.
2. Decompose the signal $x_j(t)$ into its IMF components as described in Equations (26) and (22).
3. Construct the analytical signal for each IMF/modal component using HT method described in Equation (9).
4. Obtain the phase angle of the analytic signal and then obtain the instantaneous frequency from Equation (14).
5. Obtain the log amplitude function of the analytic signal; perform least squares line fit to the function (which will be a decreasing function fluctuating about a line and not necessarily linear at all times). Then using Equation (43) compute the slope and damping ratio.

As described in earlier sections the ability of the EMD/HT method to identify the instantaneous frequency in real time is used for controlling and tuning the STMD [37] in Section 6. Next the experimental results from model tests of a three-story model with STMD are presented and analyzed using proposed EMD/HT method.

3.1. System identification tests of scaled three-story model with STMD

The 1:10 scale three-story model with a total weight of 1000 lbs, shown in Figure 3, is used for system identification study based on the proposed EMD/HT algorithm. Time axis is scaled by $\sqrt{10}$ from the prototype scale for this study. The identified frequencies of the model 3DOF structure (without the STMD) are 4.9, 18.8, and 33.9 Hz for the three modes, respectively. The first mode frequency of the original model was 5.5 Hz and was reduced to 4.9 Hz due to damage during testing, the other two modal frequencies remained nearly the same. At the prototype scale the three modal frequencies are 1.75, 5.9, and 10.7 Hz, respectively.

The model was subjected to white noise base excitation using a shaking table. The table and floor accelerations, and floor displacements were recorded. The identified displacement transfer function (TF) of 3DOF (without the STMD) is shown in Figure 5. The identified frequencies of the 3DOF are 4.9, 18.8, and 33.9 Hz and the identified damping ratios are approximately 1.9, 1.7, and 1.1% in the three modes, respectively. The recorded TF of the 3DOF is also shown in Figure 5 in comparison with the TF of the 4DOF (with STMD) obtained by an analytical model. The STMD is tuned perfectly to the first mode frequency of 4.9 Hz. The computed frequencies of the 4DOF analytical model with STMD are 4.5, 5.5, 18.8, and 33.9 Hz and the damping ratios are 1.9, 1.7, 1.0, and 1.1% in the four modes, respectively. The recorded and computed acceleration TF of the 4DOF with STMD is shown in Figure 6. Attempts to identify

DOI: 10.1002/stc

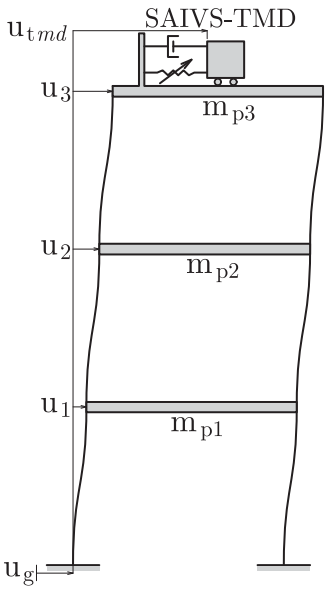

Figure 3. Three-story Building with SAIVS-TMD or STMD.

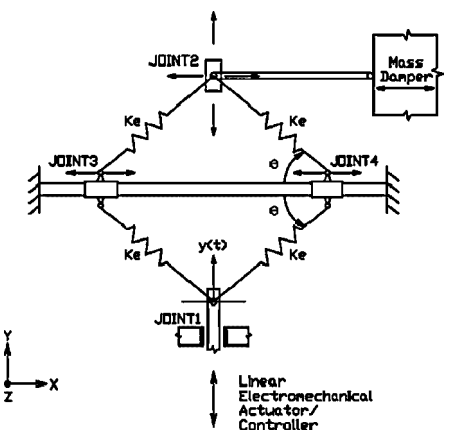

Figure 4. STMD based on SAIVS device.

the closely spaced first two modes of the 4DOF system using either the displacement or acceleration TF were not successful due to noise and averaging in the Welch's method used to identify the TF. The recorded TF of the 4DOF system shown in Figure 6 has two sharp peaks at 4.5 and 5.5 Hz. These two closely spaced modes average to approximately 4.9 Hz and appear as a single peak in the identified 4DOF TF, similar to the identified 3DOF TF shown in Figure 5, due to averaging in Welch's method used for estimating the TF. This problem is overcome by using the EMD/HT system identification technique that can identify the closely spaced modes, which is described next.

DOI: 10.1002/stc

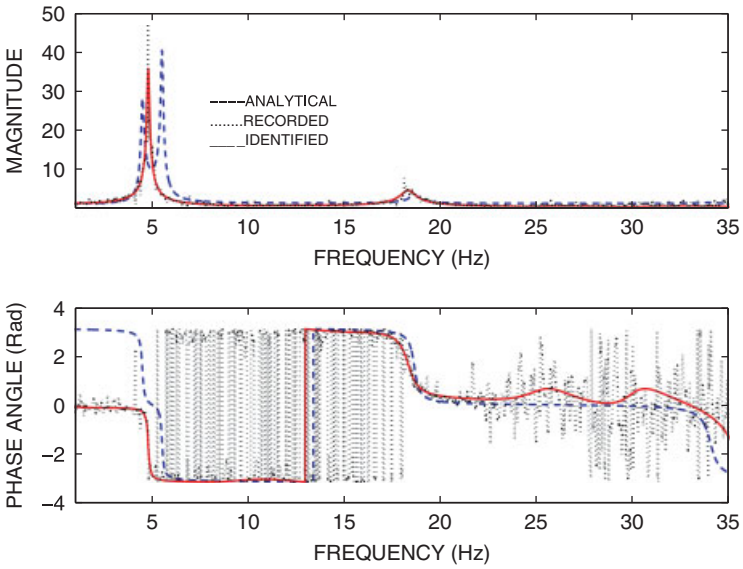

Figure 5. Displacement transfer function.

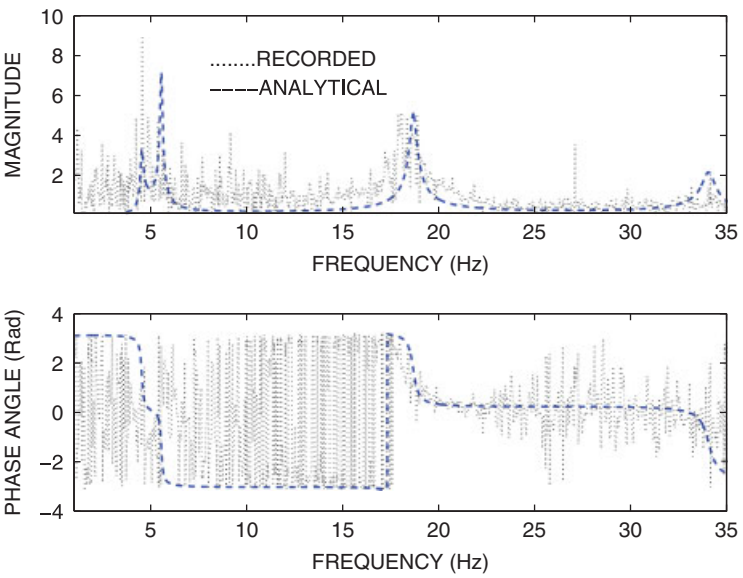

Figure 6. Acceleration transfer function.

3.2. Free vibration test results

The three-story scaled model with the STMD, tuned to the first mode frequency of 4.9 Hz, is subjected to free vibration tests. The third floor of the model is pulled and released suddenly and the third floor displacement and acceleration responses are measured. The acceleration data is

DOI: 10.1002/stc

then analyzed using EMD/HT to extract instantaneous frequency and damping ratios of the four modes as per the procedure described earlier in this section. The free vibration acceleration response of the third floor is shown in Figure 7(a) and the Fourier spectrum is shown in Figure 7(b). The first three modes are not evident in the Fourier spectrum; however, the fourth mode at 33.7 Hz is evident as its acceleration dominates the free vibration.

The third floor acceleration response is decomposed into its IMF components using EMD. The EMD method is capable of extracting all the four vibration frequencies and damping ratios from a single measurement of the acceleration response time history based on the procedure outlined before. The signal is decomposed into totally 6 IMFs; the first four are shown in Figure 8 and the rest of discarded as they are small and below the threshold. Based on the system identification procedure presented earlier, modal frequencies and damping ratios are identified using linear least squares fit as shown in Figure 9. The modal frequencies and damping ratios obtained are shown in Table I. The EMD/HT results match with the analysis results, except for the damping in the first two modes, wherein the damping due to friction in STMD that exists in the actual system and observed in the experiments is not accounted for in the linear analytical model presented in this section, while calculating the damping ratios. This additional frictional damping of approximately 3% is accounted for separately in the nonlinear time-varying analytical model to be outlined in Sections 4, 5, and 6.

3.3. White noise test results

The three-story structure with the STMD is subjected to white noise excitation (WNE) using a shaking table. The measured third floor acceleration response is shown in Figure 10(a). EMD/HT analysis is performed on the measured response and the IMF components extracted are

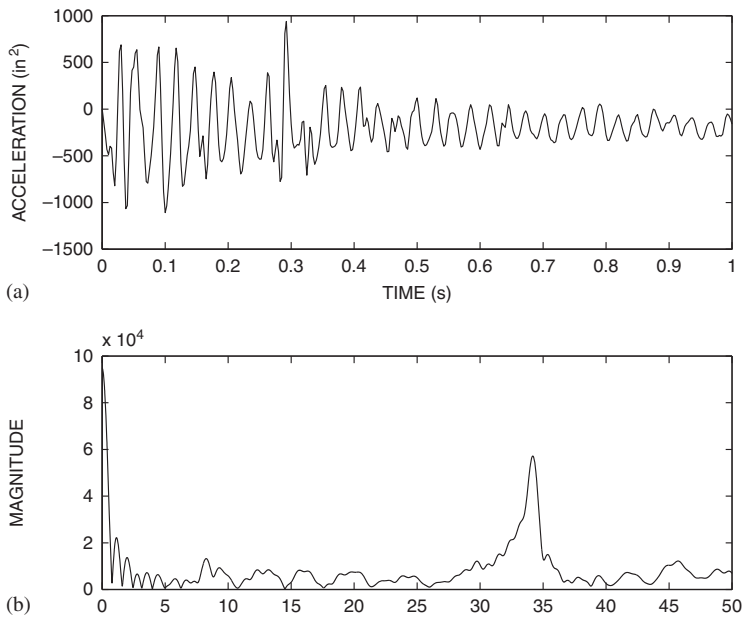

Figure 7. Free vibration third floor acceleration and FFT.

DOI: 10.1002/stc

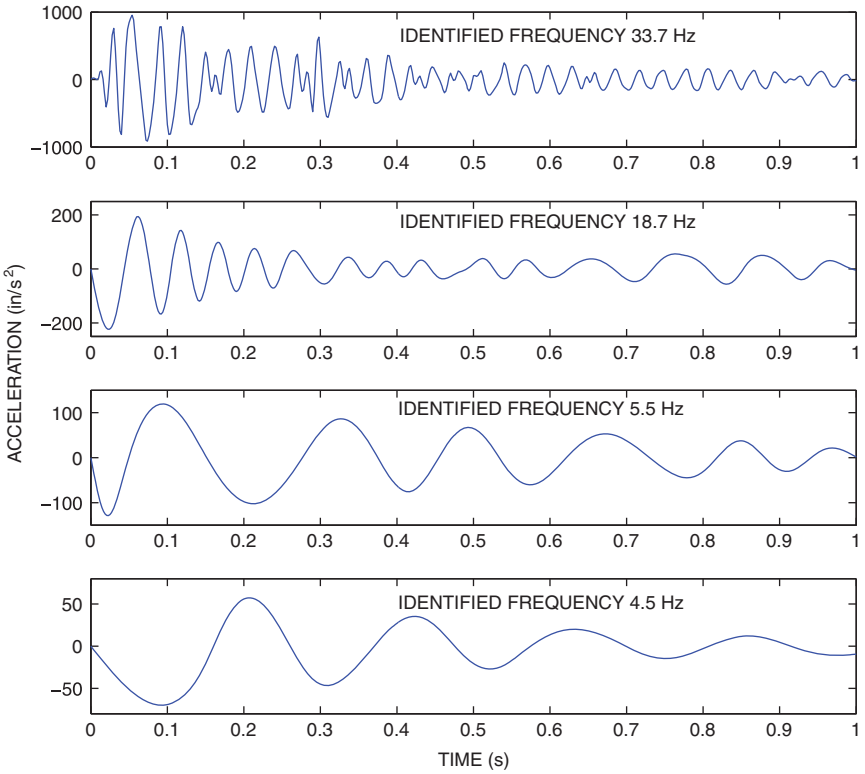

Figure 8. IMF components of the third floor acceleration.

shown in Figures 10(b)–(e). The instantaneous frequencies and damping ratios obtained are summarized in Table I. The log and phase curves for the white noise case fluctuate and are not as linear as in the free vibration case, shown in Figure 9; however, the least squares fit results in a linear estimate. It is interesting to note that counting of cycles both in free vibration (Figure 8) and white noise case (Figure 10) reveals that the estimated frequencies are reasonably accurate. The frequency and damping ratio estimates for the white noise case, shown in Table I, are the same as in the free vibration case. The estimated instantaneous frequencies are used for tune the STMD in Section 6.

4. SAIVS

SAIVS has been developed by the author and studied analytically and experimentally [13,14]. The novelty of the SAIVS system lies in its continuous and smooth switching of stiffness. The SAIVS system has been integrated into a (1) single degree of freedom system [14], STMD [31,32,35], and (3) base isolated building [48,49], studied in detail analytically and experimentally.

The SAIVS device, shown in Figure 11, consists of four spring elements arranged in a plane rhombus configuration with pivot joints at the vertices. A linear electromechanical actuator configures the aspect ratio of the rhombus configuration of SAIVS device. The aspect ratio changes between the fully closed (joint 1 and 2 are in closest position) and open configurations

DOI: 10.1002/stc

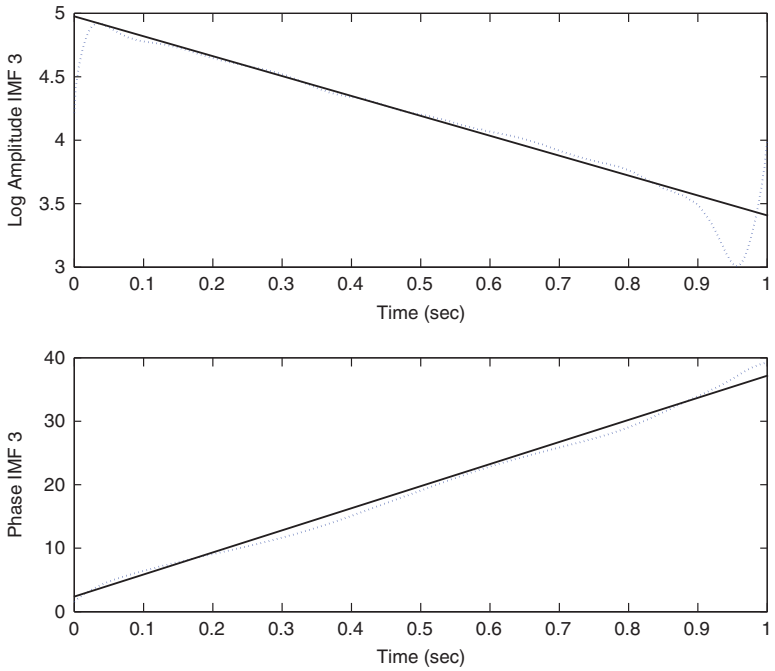

Figure 9. Log amplitude of IMF3 and phase angle (rad).

Table I. Frequencies and damping ratios of scaled three-story model with STMD.

	Free vibration tests		White noise tests	
Mode	Identified frequency (Hz)	Identified damping ratio (%)	Identified frequency (Hz)	Identified damping ratio (%)
1	4.5	4.6	4.5	4.6
2	5.5	4.4	5.5	4.4
3	18.7	1.0	18.7	1.0
4	33.7	1.1	33.7	1.0

(joint 3 and 4 are in closest position), leading to maximum and minimum stiffness, respectively. A control algorithm and controller are used to regulate the linear electromechanical actuator. The power required by the actuator to change the aspect ratio of the device is nominal. The variable stiffness of the SAIVS device is described by:

$$k(t) = k_e \cos^2(\theta(t)) \tag{44}$$

where $k(t)$ = time varying stiffness of the device, k_e = the constant spring stiffness of each spring element, and $\theta(t)$ = time varying angle of the spring elements with the horizontal in any position of the device. The SAIVS device has maximum stiffness in its fully closed ($\theta(t) = 0$) and minimum stiffness in its fully open position ($\theta(t) \sim \pi/2$). The device can be positioned in any configuration, changing its stiffness continuously, independently and smoothly between maximum and minimum stiffness, as shown in force-displacement loops in Figure 12.

DOI: 10.1002/stc

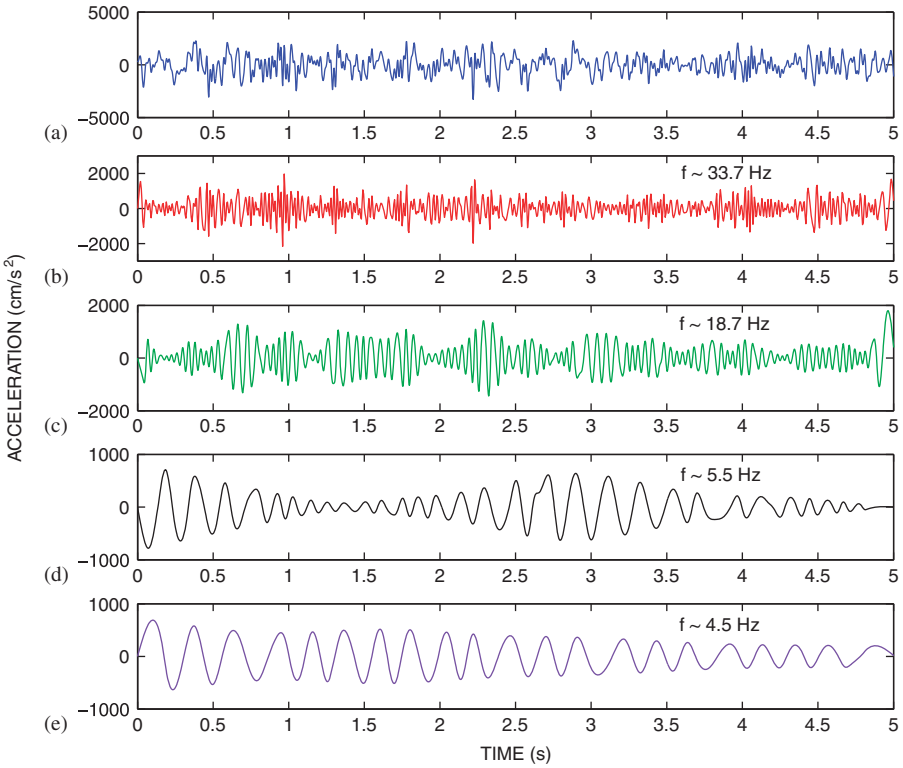

Figure 10. Third floor acceleration and its IMF components.

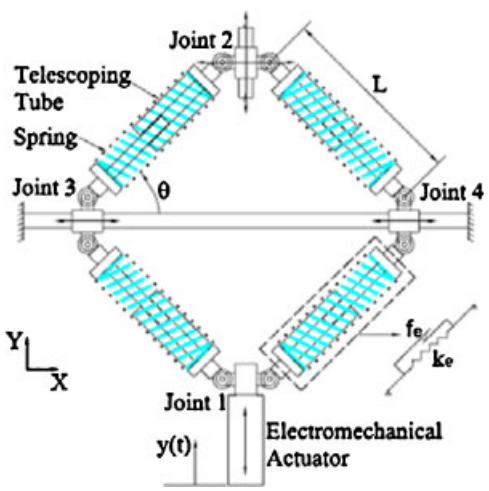

Figure 11. SAIVS device.

DOI: 10.1002/stc

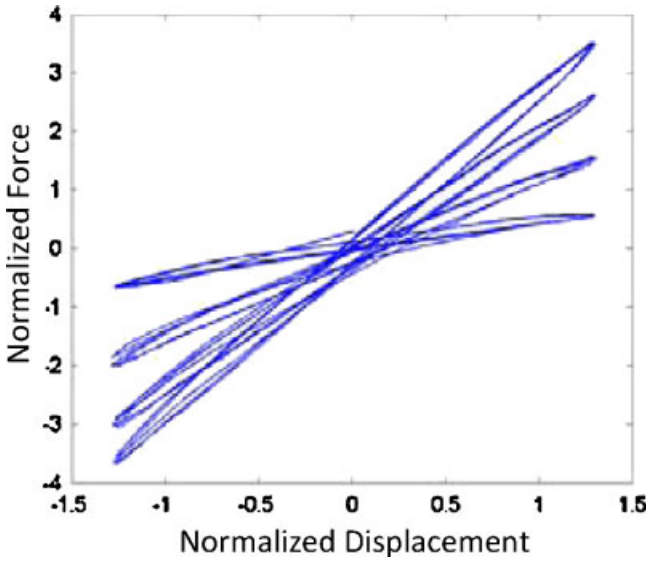

Figure 12. Force–displacement behavior of SAIVS device.

The device also develops friction forces in the springs' arms, which are telescopic, and at joints 1–4. The analytical model can be formulated to represent these forces. The force $f_{sv}(t)$ developed by the SAIVS device at any time, for a specific device position, is given as:

$$f_{sv}(t) = f_r(t) + f_f(t, \dot{u}) \tag{45}$$

where f_r is the restoring force due to spring deformation and f_f is the frictional force in the telescoping tubes; $u(t)$ is the displacement at joint 2 in the X direction. The restoring force f_r is given as

$$f_r(t) = \{k_e \cos^2 \theta(t)\} u(t) \tag{46}$$

where k_e is the constant stiffness of single spring element, $\theta(t)$ is the time varying angle of the spring elements with the horizontal for any given device position

$$\theta(t) = \sin^{-1}\left(\alpha - \frac{y(t)}{\beta}\right) \tag{47}$$

with α being a non-dimensional constant $\left(\alpha > \frac{y(t)}{\beta}\right)$ and $\beta = 4\,\text{in}$ is the dimension of an individual spring element and $y(t)$ is the displacement of joint 1 or the linear electro-mechanical actuator, which is controlled to be less than β [48].

5. MATHEMATICAL FORMULATION OF LTV SYSTEMS WITH STMD

Consider a MDOF primary system with an attached secondary mass connected at the top, by a variable stiffness spring and dashopt (i.e. SAIVS device), with an STMD as shown in Figure 3. The primary structure has a mass matrix, $\mathbf{M}_p$, a stiffness matrix, $\mathbf{K}_p$, and a damping, $\mathbf{C}_p$, whereas the STMD is composed of a secondary mass, m_s, which is connected to the primary system by a

DOI: 10.1002/stc

spring of stiffness, $k_s + k_{sv}(t)$, and a dashpot of viscous damping coefficient, $c_s + c_{sv}(t)$, as shown in Figure 3.

The equations of motions of a MDOF system with a STMD connected at the top are as follows,

$$\mathbf{M}_p \ddot{\mathbf{U}}_p + \mathbf{C}_p \dot{\mathbf{U}}_p + \mathbf{K}_p \mathbf{U}_p = -\mathbf{R} f_{sv}(t) + \mathbf{F}_p + \mathbf{R}(c_s \dot{u}_r + k_s u_r) \tag{48}$$

where $f_{sv}(t) = c_{sv}(t)\dot{u}_r + k_{sv}(t)u_r$ and $\mathbf{R} = [1 \;\; 0 \;\; \cdot \;\; \cdot \;\; \cdot \;\; 0]^{\mathrm{T}}$.

$$\ddot{\mathbf{U}}_p = -\mathbf{M}_p^{-1}\mathbf{K}_p\mathbf{U}_p - \mathbf{M}_p^{-1}\mathbf{C}_p\dot{\mathbf{U}}_p - \mathbf{M}_p^{-1}\mathbf{R}f_{sv}(t) + \mathbf{M}_p^{-1}\mathbf{F}_p + \mathbf{M}_p^{-1}\mathbf{R}(c_s\dot{u}_r + k_s u_r) \tag{49}$$

$$m_s \ddot{u}_s = f_{sv}(t) + F_s \tag{50}$$

$$m_s(\ddot{u}_{pn} + \ddot{u}_r) = f_{sv}(t) + F_s \tag{51}$$

$$\ddot{u}_r = \frac{1}{m_s} f_{sv} + \frac{1}{m_s} F_s - \ddot{u}_{pn} \tag{52}$$

$$\ddot{u}_r = \frac{1}{m_s} f_{sv} + \frac{1}{m_s} F_s + \mathbf{R}^{\mathrm{T}}\mathbf{M}_p^{-1}\mathbf{K}_p\mathbf{u}_p + \mathbf{R}^{\mathrm{T}}\mathbf{M}_p^{-1}\mathbf{C}_p\dot{\mathbf{u}}_p + \mathbf{R}^{\mathrm{T}}\mathbf{M}_p^{-1}\mathbf{R}f_{sv} + \mathbf{R}^{\mathrm{T}}\mathbf{M}_p^{-1}\mathbf{R}(c_s\dot{u}_r + k_s u_r) - \mathbf{R}^{\mathrm{T}}\mathbf{M}_P^{-1}\mathbf{F}_p \tag{53}$$

In state space form

$$\dot{\mathbf{X}} = \mathbf{A}\mathbf{X} + \mathbf{B}\mathbf{F}_{sv}(t) + \mathbf{E}\mathbf{F} \tag{54}$$

where

$$\mathbf{X} = \begin{Bmatrix} u_{\mathrm{p}} \\ u_{\mathrm{r}} \\ \dot{\mathbf{u}}_{\mathrm{p}} \\ \dot{u}_{\mathrm{r}} \end{Bmatrix}; \quad \mathbf{A} = \begin{bmatrix} \mathbf{O}_{nn} & \mathbf{O}_{n1} & \mathbf{I}_{nn} & \mathbf{O}_{n1} \\ \mathbf{O}_{1n} & \mathbf{O}_{11} & \mathbf{O}_{1n} & \mathbf{I}_{11} \\ -\mathbf{M}_p^{-1}\mathbf{K}_p & -\mathbf{M}_p^{-1}\mathbf{R}k_s & -\mathbf{M}_p^{-1}\mathbf{C}_p & -\mathbf{M}_p^{-1}\mathbf{R}c_s \\ \mathrm{R}^{\mathrm{T}}\mathbf{M}_p^{-1}\mathbf{K}_p & \mathbf{R}^{\mathrm{T}}\mathbf{M}_p^{-1}\mathbf{R}k_s & \mathbf{R}^{T}\mathbf{M}_p^{-1}\mathbf{C}_p & \mathbf{R}^{\mathrm{T}}\mathbf{M}_p^{-1}\mathbf{R}c_s \end{bmatrix}$$

$$\mathbf{B} = \begin{bmatrix} \mathbf{O}_{nn} & \mathbf{O}_{n1} \\ \mathbf{O}_{1n} & \mathbf{O}_{11} \\ \mathbf{O}_{nn} & -\mathbf{M}_p^{-1}\mathbf{R} \\ -\mathbf{R}^{\mathrm{T}}\mathbf{M}_p^{-1} & \mathbf{R}^{\mathrm{T}}\mathbf{M}_p^{-1}\mathbf{R} + \dfrac{1}{m_s} \end{bmatrix}; \quad \mathbf{F}_{sv} = \begin{bmatrix} \mathbf{O}_{n1} \\ f_{sv}(t) \end{bmatrix}; \quad \mathbf{E} = \begin{bmatrix} \mathbf{O}_{nn} & \mathbf{O}_{n1} \\ \mathbf{O}_{1n} & \mathbf{O}_{11} \\ \mathbf{M}_p^{-1} & \mathbf{O}_{n1} \\ -\mathbf{R}^{\mathrm{T}}\mathbf{M}_p^{-1} & \dfrac{1}{m_s} \end{bmatrix}$$

$$\mathbf{F} = \begin{bmatrix} \mathbf{F}_p \\ F_s \end{bmatrix}$$

It is the previous section it was shown in Equation (45) that the SAIVS device force

$$f_{sv}(t) = f_r(t) + f_f(t, \dot{u}) \tag{55}$$

where $f_r(t) = k_e \cos^2\theta(t)u(t)$ with k_e being the stiffness of one of the four springs, $\theta(t)$ is a time-varying angle of the spring elements with the horizontal, and f_f being the frictional forces in the device [48].

DOI: 10.1002/stc

The equations are solved using a predictor-corrector solution algorithm, which is a modified form of method of successive approximation.

6. NEW CONTROL ALGORITHMS FOR MDOF WITH STMD

STMD consists of the variable stiffness spring or SAIVS device connected to a mass on top of the three-story structure as shown in Figure 4. The mass ratio μ of the TMD and the STMD is chosen to be 1%. The simulated frequency response curves (showing the dynamic magnification factor [DMF], which is the dynamic displacement normalized with respect to static displacement of the primary mass, as a function of excitation frequency normalized by first mode frequency) in the case of TMD and STMD (where the frequency of the STMD is tuned to the excitation frequency; interested reader can find further details in Nagarajaiah and Sonmez [32]) are shown in Figure 13, for different damping ratios. It is clearly evident that the STMD is more effective than a TMD especially for lower damping ratios—smaller the damping the superior the performance of the STMD. In Figure 14 DMF as a function of damping ratio of the TMD/STMD is shown; the optimal damping is nearly seven percent and when the STMD damping approaches approximately 8% the response is similar to TMD. In Figure 13(d) with damping ratio 10% the effectiveness of both the TMD and STMD is reduced; the DMF is clearly above the case with damping ratio of 7% in Figure 13(c) and above the case with damping ratio of 4%

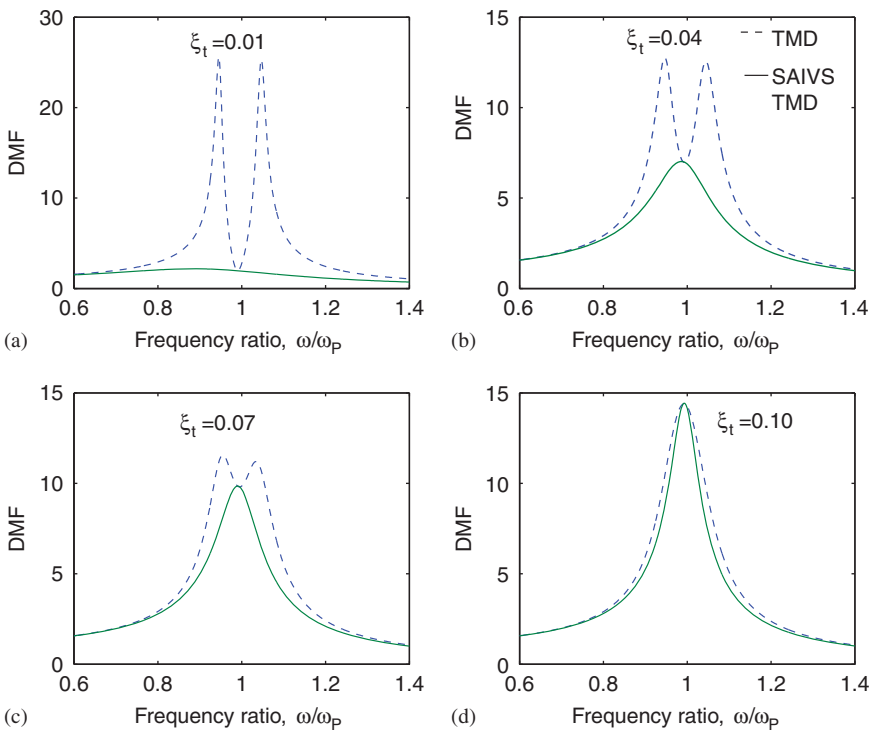

Figure 13. Frequency response curves for TMD/STMD for various damping.

DOI: 10.1002/stc

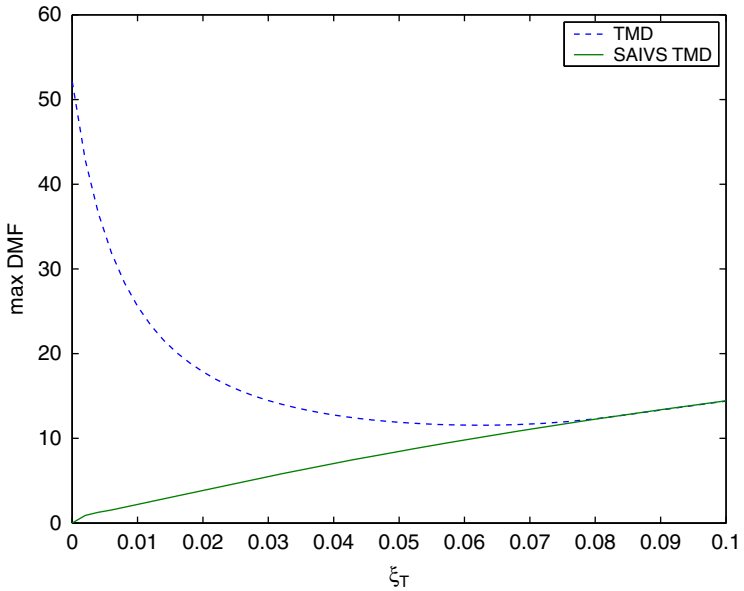

Figure 14. Optimal damping.

in Figure 13(b). In essence, increasing damping beyond the optimal is not be beneficial in this case. Recall our discussion regarding use of variable damping for tuning STMD's in Section 1.2? Would it be judicious to adjust damping in light of the requirement of optimal damping and tuning as well? It certainly seems more desirable to tune using stiffness rather than damping, unless there are other compelling reasons such as stroke restrictions, etc.

From Figure 13 it is also seen that the effectiveness of the STMD is maximized when the frequency of the STMD is between $0.7f_{p1}$ and $1.3f_{p1}$, where f_{p1} is the fundamental frequency of mode p_1 of the MDOF primary system. The frequency variation of the STMD, therefore, is chosen to be $0.7f_{p1} < f_s < 1.3f_{p1}$. In the fully open position the frequency of the STMD is $0.7f_{p1}$. When the device is fully closed the frequency of the STMD is $1.3f_{p1}$.

Next, new control algorithms based on EMD/HT technique and STFT are developed for selecting the stiffness of the STMD when the structure is subjected to sine sweep or white noise or ground excitations.

6.1. New algorithm using empirical mode decomposition

The new EMD/HT control algorithm block diagram is shown in Figure 15. The stiffness of the SAIVS device is varied continuously to tune the STMD. The instantaneous frequency is identified based on EMD and HT algorithm described earlier (Equations (22)–(43)). The displacement of the top floor is the only feedback used in the instantaneous frequency algorithm. Once the dominant instantaneous frequency at which the system with STMD is responding is identified based on the procedure outlined earlier, the stiffness of the STMD is adapted to tune to the dominant frequency and maximize the response reduction.

DOI: 10.1002/stc

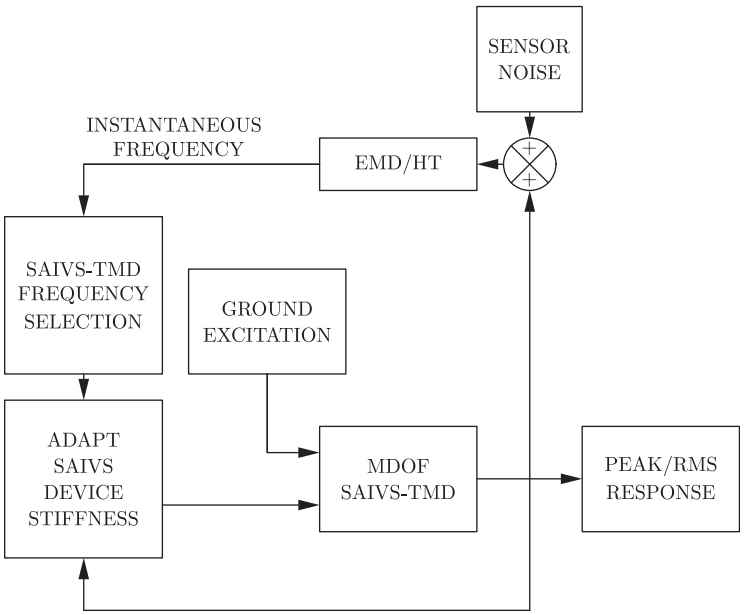

Figure 15. EMD/HT control algorithm.

The EMD/HT control algorithm developed to choose the stiffness of the STMD from the frequency, f_{STMD}, is as the follows:

1. A moving window of 512 time steps, $\Delta t = 0.005$ s, or 2.56 s is chosen to determine the EMD intrinsic mode components, imf_i, from the top floor displacement; only the first three components, $\mathrm{imf}_{1,2,3}$, are used, since they represent the first three dominant modal frequencies that the structure with STMD is responding at.
2. The instantaneous frequency of each component, $\mathrm{imf}_{1,2,3}$, is identified and updated at every $\Delta t_{\mathrm{EMD}} = 0.02$ s using HT.
3. The dominant frequency, f^{d}_{imf}, in each window is identified from $\mathrm{imf}_{1,2,3}$.
4. If the dominant frequency of f^{d}_{imf} is in the range $0.7f_{p1} < f^{d}_{\mathrm{imf}} < 1.3f_{p1}$, then $f_{\mathrm{STMD}} = f^{d}_{\mathrm{imf}}$, else go to next step.
5. Set f_{STMD} to the optimum value f_{TMD}.

6.2. New algorithm using STFT

The control algorithm block diagram is shown in Figure 15, except that the EMD/HT block is replaced by STFT block. A new STFT control algorithm is developed to retune the STMD. STFT controller is effective in both monocomponent sine-sweep excitations, as well as in multicomponent non-stationary earthquake excitations. The instantaneous frequency is identified based on STFT algorithm described earlier (Equations (15)–(21)). The displacement of the top floor is the only feedback used in the instantaneous frequency algorithm. Once the dominant instantaneous frequency at which the system with STMD is responding is identified

DOI: 10.1002/stc

based on the procedure outlined earlier, the stiffness of the STMD is adapted to tune to the dominant frequency and maximize the response reduction.

The STFT control algorithm developed to choose the stiffness of the STMD is as follows:

1. A moving window of 128 time steps, $\Delta t = 0.005\,\text{s}$, is chosen to determine the STFT dominant frequency from the top floor displacement feedback.
2. The dominant frequency, f_d, in each window is identified.
3. If the dominant frequency of f_d is in the range $0.7f_{p1} < f_d < 1.3f_{p1}$, then $f_{\text{STMD}} = f_d$, else go to next step.
4. Set f_{STMD} to the optimum value f_{TMD}.

6.3. Numerical example: prototype 3 story building with STMD

The numerical example considered in this section is the prototype of three-story building, described earlier in Section 3.1, shown in Figure 3. The natural frequencies of the 3DOF system (without STMD) at prototype scale are 1.75, 5.9, and 10.7 Hz. The proportional damping ratios for all the three modes are assumed to be 1%. In addition, the frictional damping in the SAIVS device of STMD, equivalent to approximately 3%, is accounted for using the SAIVS analytical model in Equations (45) and (55). The linear TF of the 4DOF system with STMD is computed. The frequencies of the 4DOF system are 1.6, 1.96, 5.9, and 10.7 Hz in the four modes, respectively. The TF of the first two modes of the prototype structure considered is shown in Figure 16.

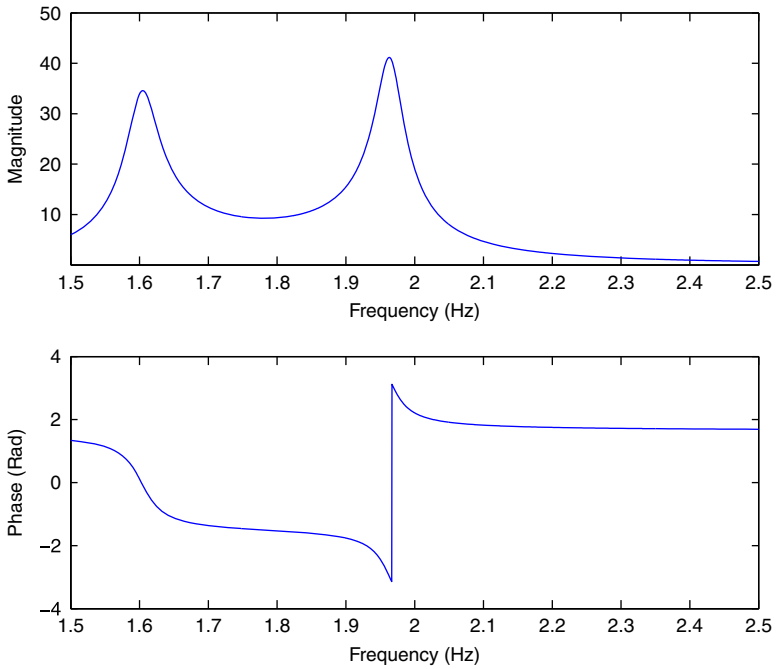

Figure 16. TF of three-story prototype structure.

DOI: 10.1002/stc

6.4. *Results for sine-sweep ground excitation*

The effectiveness of the STMD with the new EMD/HT control algorithm is evaluated by exciting the three-story building with a monocomponent sine-sweep ground excitation (SSE) in the range 1.25–2.2 Hz, to excite the 4DOF system in the range of $0.7f_{p1} < f_s < 1.3f_{p1}$, as shown in Figure 19. Simulations are carried out with the TMD tuned optimally and with 7% optimal damping. The comparison of the normalized third story displacement for TMD and STMD cases is shown in Figure 17(a) and the normalized acceleration is shown in Figure 17(b). It is evident that the STMD reduces the response, when compared to TMD case. Additionally, the peaks of the time history plots nearly match with the DMF curves in Figure 13(c). In Figure 17, in the TMD case the first peak (DMF $\sim$ 11) occurs at $\sim$63 s, when the excitation frequency crosses the first mode frequency of 1.6 Hz and second peak (DMF $\sim$11) occurs at $\sim$ 72 s when the excitation frequency crosses the second mode frequency of 1.95 Hz; in the STMD case the only peak (DMF $\sim$10) occurs at $\sim$67 s.

Next we show the response of a perfectly tuned TMD system with 4% damping (the damping observed in Table I); henceforth, all simulations are performed for 4% nominal damping in TMD/STMD. The comparison of the normalized third story displacement and acceleration is shown in Figure 18. The effectiveness of the controller in retuning STMD and achieving response reduction is clearly evident in Figure 18. In Figure 18, in the TMD case the first peak (DMF $\sim$13) occurs at $\sim$63 s, when the excitation frequency crosses the first mode frequency of 1.6 Hz and second peak (DMF $\sim$13) occurs at $\sim$72 s when the excitation frequency crosses the second mode frequency of 1.95 Hz; in the STMD case the only peak (DMF $\sim$6.5) occurs at $\sim$67 s. The STMD reduces the primary system response by nearly 50%.

Figure 19 shows the effectiveness of the new control algorithm in tracking the dominant response instantaneous frequency due to sinsweep excitation, which is used for adjusting the

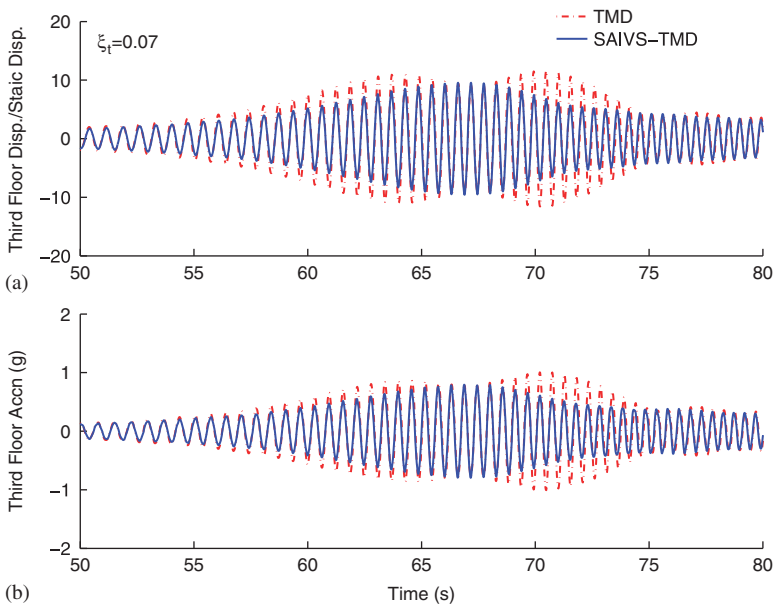

Figure 17. TMD with optimal 7% damping: tuned case (SSE).

DOI: 10.1002/stc

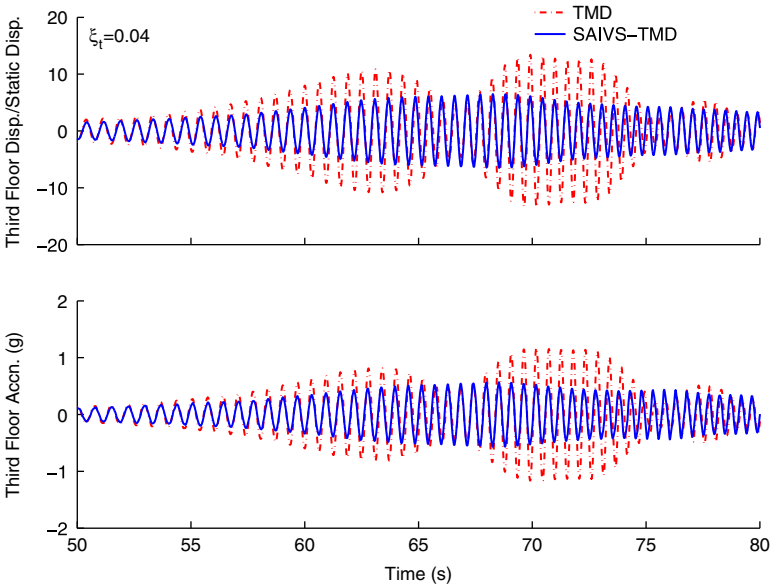

Figure 18. Tuned TMD with 4% damping (SSE).

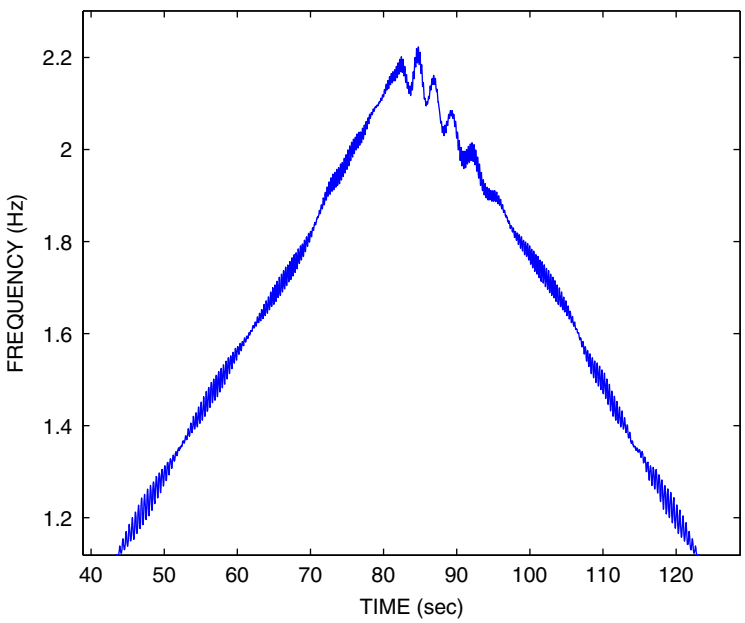

Figure 19. Frequency tracking of STMD: tuned case (SSE).

stiffness of SAIVS continuously to tune the STMD. Figure 20 shows the force-displacement of the STMD adapting its stiffness to the changing instantaneous frequency of response; whereas, the TMD stiffness remains fixed. The force-displacement in Figure 20 is nonlinear due to friction

DOI: 10.1002/stc

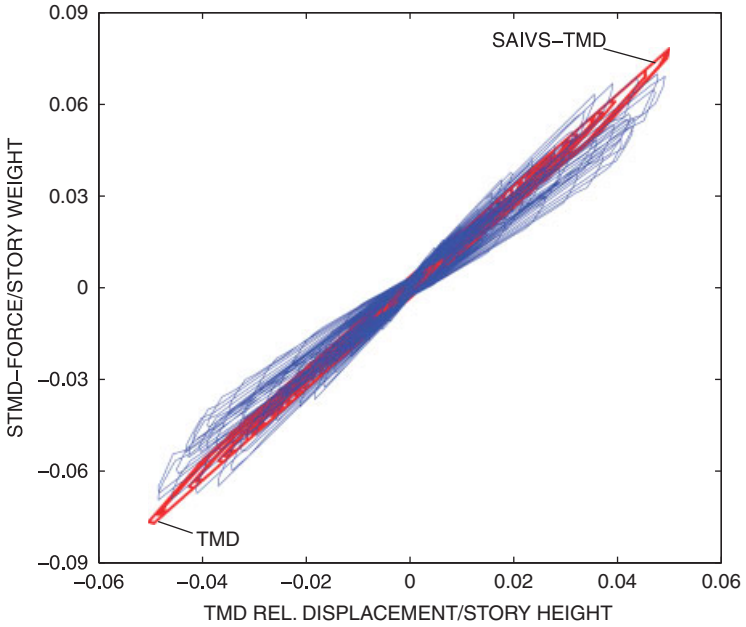

Figure 20. Force–displacement loop: tuned case (SSE).

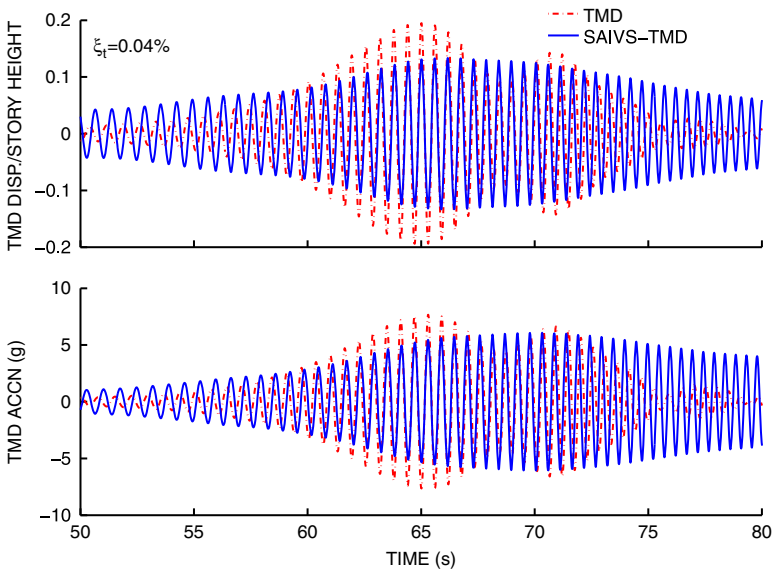

Figure 21. TMD and STMD response: tuned case (SSE).

in the SAIVS device (Equations (45) and (55)). Figure 21 shows the response of the TMD and STMD; it is evident that the STMD is able to achieve the response reduction without increasing its displacement as compared to the TMD. Hence, the EMD/HT controller presented is effective.

DOI: 10.1002/stc

The STFT control algorithm yields similar results as the EMD/HT control algorithm and is equally effectiveness; thus, not repeated in the interest of space.

As discussed earlier, the TMD is sensitive to tuning ratio; its effectiveness is reduced when it is mistuned even just by 5%. To demonstrate the sensitivity we present the results of 5% mistuned case in Figure 22. The normalized third floor response for 5% mistuning, shown in Figure 22, confirms that the STMD is still effective as it is able to retune and reduce the response, whereas the TMD is unable to reduce the response as much as the case with optimal tuning. In Figure 22 the TMD case has only one peak (DMF $\sim$ 15) that occurs at $\sim$70 s, when the excitation frequency crosses the frequency of $\sim$1.75 Hz (indicating a single peak instead of the two peaks in the TF because the system behaves like the case without STMD) and in the STMD case the only peak (DMF $\sim$6.5) occurs at $\sim$70 s; the STMD continues to reduce the response in excess of 50% due to retuning.

6.5. Results for white noise ground excitation

The three-story building with the STMD described earlier is excited by a multi-component WNE to evaluate the effectiveness of the new EMD/HT and STFT algorithms. Comparison of the simulated normalized third floor displacement and acceleration in Figures 23 indicate the effectiveness of the STMD in reducing the response. Comparison of the power spectral density (PSD) of the third floor acceleration in Figure 24 shows that the STMD reduces the response when compared to the TMD case over wide frequency range; particularly, if the response due to the excitation is near the natural fundamental frequency of the primary structure, then the STMD is able to adaptively reduce the response significantly.

The response to WNE (broadband excitation) is shown in Figure 25 for the case with 5% mistuning. The normalized displacement and acceleration response shown in Figure 25 indicate that the response is still reduced in the STMD case, due to retuning, when compared to the TMD case. The PSD of the third floor acceleration due to multicomponent WNE, in Figure 26,

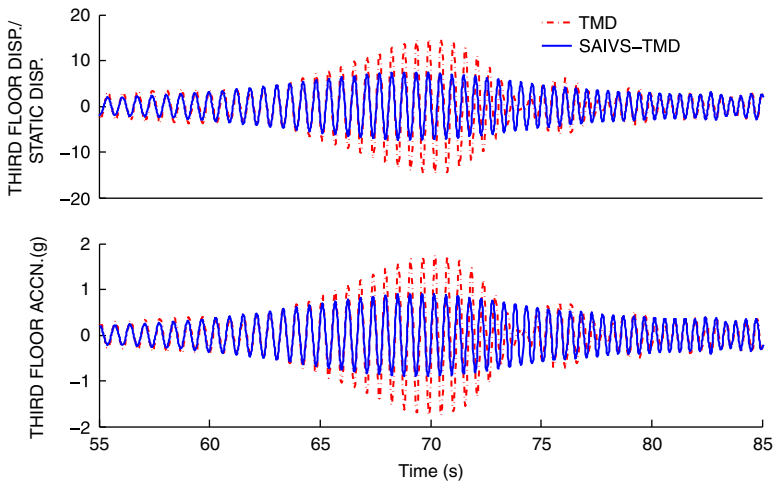

Figure 22. TMD and STMD response: mistuned case (SSE).

DOI: 10.1002/stc

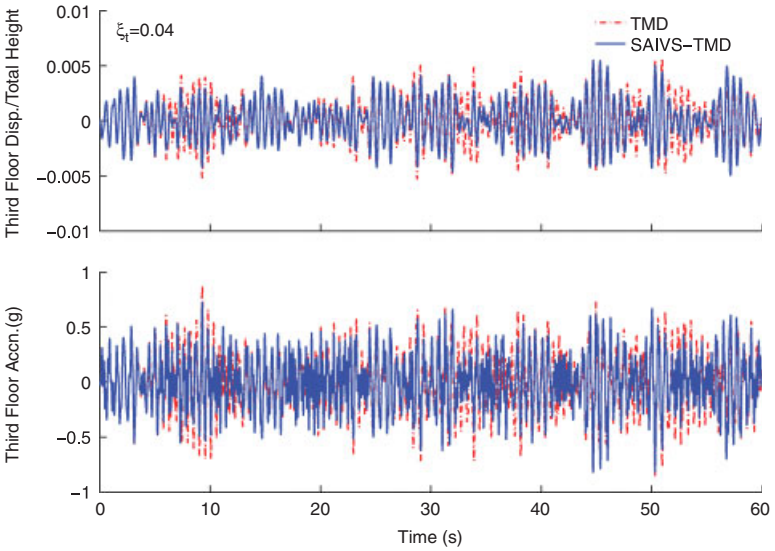

Figure 23. Response: tuned case (WNE).

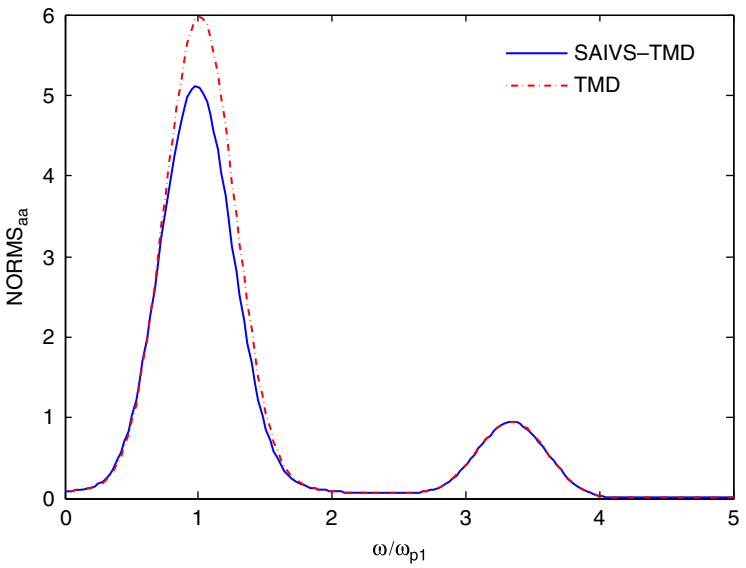

Figure 24. PSD of three-floor acceleration: tuned case (WNE).

indicates the sensitivity of the response to the mistuning of the TMD. STMD reduces the response by nearly 40%. The results confirm the robustness of the STMD.

The STFT control algorithm yields similar results as the EMD/HT control algorithm and is equally effectiveness; thus, not repeated in the interest of space.

DOI: 10.1002/stc

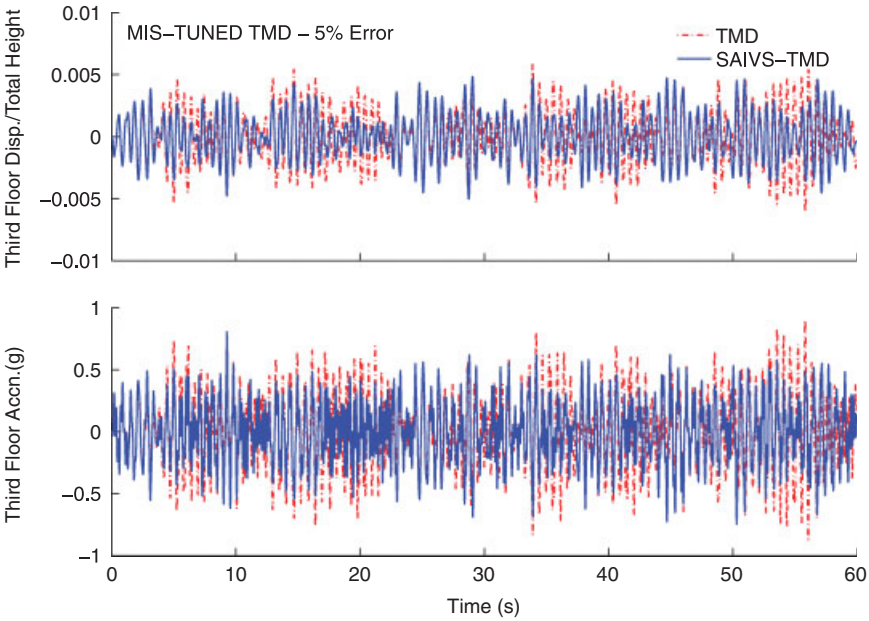

Figure 25. Response: mistuned case (WNE).

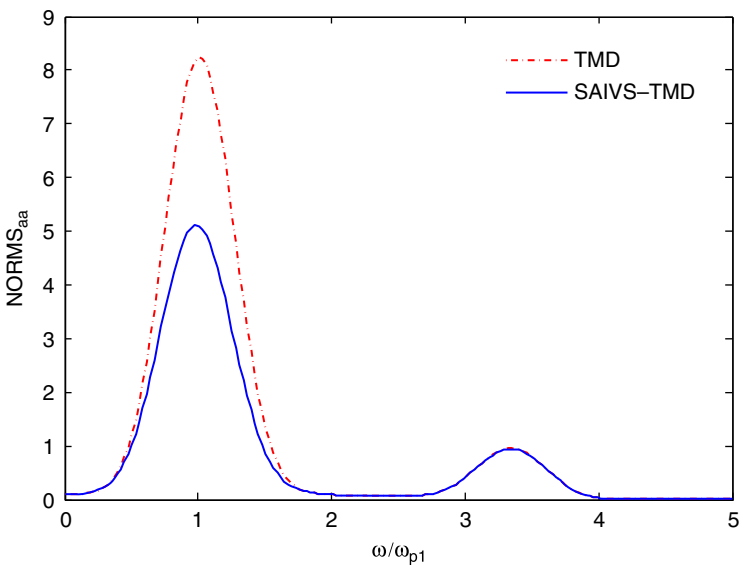

Figure 26. PSD of three-floor acceleration: mistuned case (WNE).

6.6. *Results for El centro ground motion*

The three-story building with the STMD described earlier is excited by El Centro (El-CE) earthquake excitation to evaluate the effectiveness of the new STFT algorithm under

DOI: 10.1002/stc

nonstationary excitation. Comparison of the simulated normalized third floor displacement and acceleration in Figures 27 indicates the effectiveness of the STMD in reducing the response. Comparison of the PSD of the third floor acceleration in Figure 28 shows that the response of the STMD is better than the TMD over wide frequency range; particularly, if the response due to the excitation is near the natural fundamental frequency of the primary structure, then the STMD is able to adaptively reduce the response by nearly 50%.

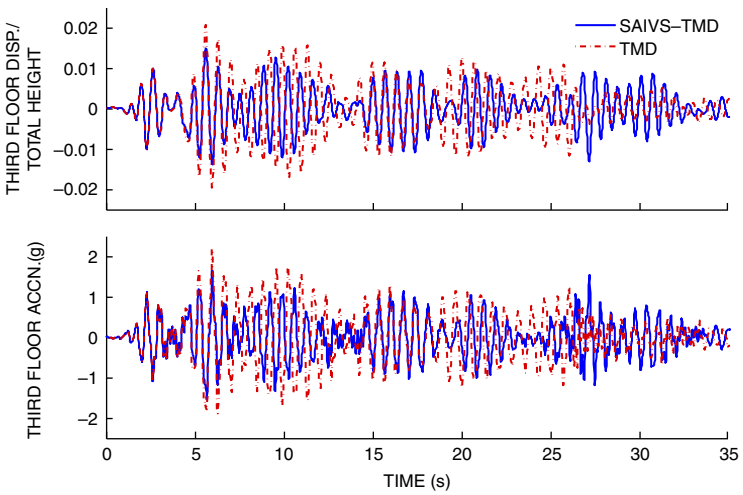

Figure 27. Response: tuned case (El-CE).

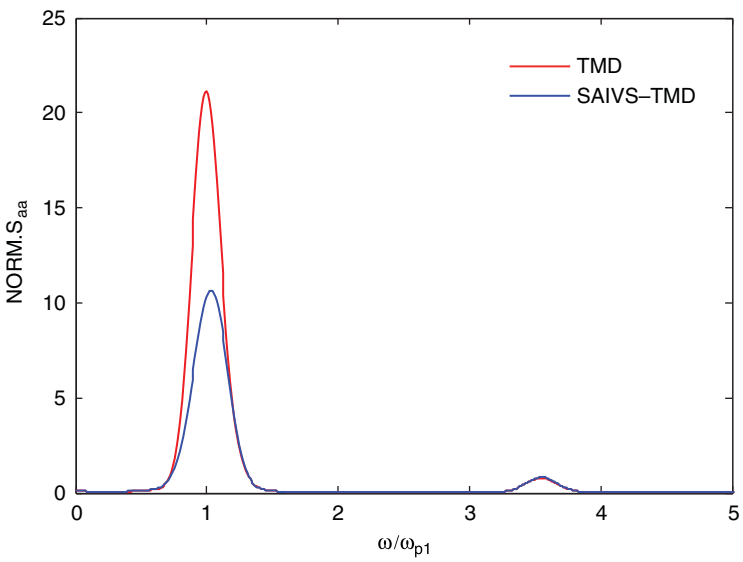

Figure 28. PSD of three-floor acceleration: tuned case (WNE).

DOI: 10.1002/stc

7. ALP STMD AND APTMD

The instantaneous natural frequency of the pendulum, $\omega = \sqrt{g/L}$, (where g is the acceleration due to gravity and L is the length of the pendulum) can easily be adjusted by changing the length of the pendulum, thus the name ALP STMD and ALP-TMD (or ALP APTMD), depending on whether length is controlled using feedback or adjusted passively. In this section we present a simple experimental evaluation of this new idea using 2DOF with ALP attached to its second floor as shown in Figure 29. The ALP is controlled using STFT algorithm to track the frequency and setting the length of the pendulum to the optimal once steady state vibration is reached. The response of the 2DOF primary structure with STMD is compared to the structure with ALP-TMD or ALP-APTMD whose length is not optimal; the lengths are set in two stages (1) non-optimal length, and (2) optimal length. It is worth noting that this is not meant to be an exhaustive study, which is beyond the scope of this paper due to space restrictions (authors will present more detailed work on ALP in a separate paper); but the demonstration of the key idea, which is very practical and easy to implement.

The candidate two story building model with ALP attached to the second floor is shown in Figure 29. The acceleration transfer function of the 2DOF is shown in Figure 30; in this case TMD mass is attached rigidly to the second floor. The natural frequencies are 2.5 and 7.0 Hz in the two modes, respectively, and the damping ratio is less than 1% in the first mode and nearly 2% in the second mode. The length of the pendulum can be adjusted by means of a servomotor shown in Figure 29(c); the shorter length ALP STMD is shown in Figure 29(a) and the longer length ALP is shown in Figure 29(b).

The optimal length of the ALP is 1.5 in (ALP frequency = 2.5 Hz), if it has to match the first mode frequency of the primary system of the 2DOF. Results of three experiments carried out under harmonic excitation of frequency 2.5 Hz are shown in Figure 31. The normalized (maximum response of one) second floor displacement response is shown in Figure 31 for three cases: (1) TMD mass fixed rigidly to the top of the structure (dotted line), (2) ALP-STMD optimally tuned at 13 s when steady-state vibration is reached (dashed line), and (3) ALP's length is adjusted

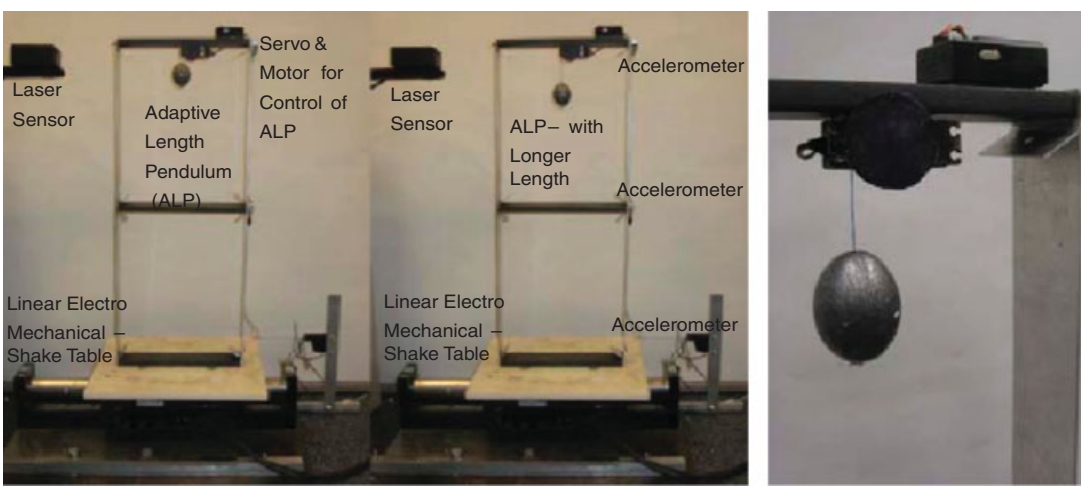

(a) (b) (c)

Figure 29. ALP TMD: (a) ALP with shorter length; (b) ALP with longer length; and (c) close up of ALP.

DOI: 10.1002/stc

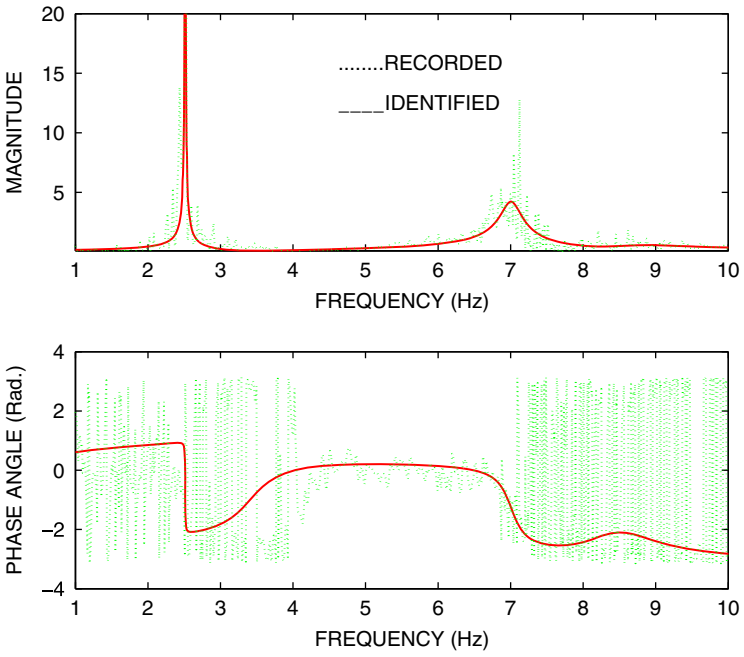

Figure 30. Acceleration TF: 2DOF.

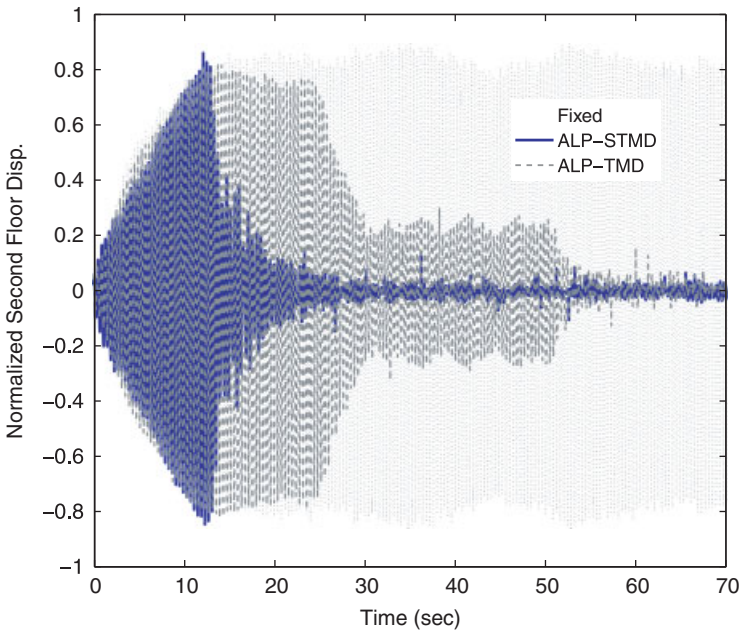

Figure 31. Top floor response: ALP-STMD.

DOI: 10.1002/stc

non-optimally (1.3 in at 25 s) in the first stage and then optimally (1.5 in at 50 s) in the second stage (full line). From the responses shown in Figure 31 it is evident that the ALP-STMD can clearly retune itself and reduce the response significantly as compared to the fixed and ALP-TMD or ALP-APTMD case; also the change in length of 0.2 in can reduce the effectiveness of the ALP-TMD. However, ALP-TMD has an advantage over a fixed length pendulum TMD, in that its length can be adjusted passively, if necessary (say when a change in primary structure frequency is detected). We present the idea APTMD next to further elaborate this idea.

7.1. Practical adaptive radius and adaptive length ALP and APTMD

A practical ALP STMD or APTMD is shown in Figure 32. Similarly an adaptive radius pendulum STMD or APTMD is shown in Figure 33, wherein the radius can be adapted either semiactively if the connector is servocontrolled or passively if the connector is mechanical and can be adjusted manually.

Another adaptive passive TMD (APTMD) developed using SAIVS device is one in which the stiffness can be adjusted passively by using a simple screw jack to change the angle of the SAIVS device, instead of the linear electro-mechanical actuator as shown in Figure 11. Such a device is fully passive and the stiffness can be changed by manually adjusting the screw jack, which does not need feedback control.

A possible adaptive radius APTMD is shown in Figure 34, wherein the concave surface on which the middle roller moves can be shaped/tuned to provide the necessary change in radius from R_1 to R_2. Also a fail safe limiting stop can be added at the end of the concave surface preventing excessive stroke.

A possible adaptive passive TMD is shown in Figure 35(a), wherein the stiffness and damping changes once the pendulum contacts the adaptive fluid spring and damper (ASD)—similar to ASD studied by the author and coworkers [50]—then further adaptation is possible. The ASD has mechanical valves that allow manual adjustment of fluid spring stiffness and damping. Another

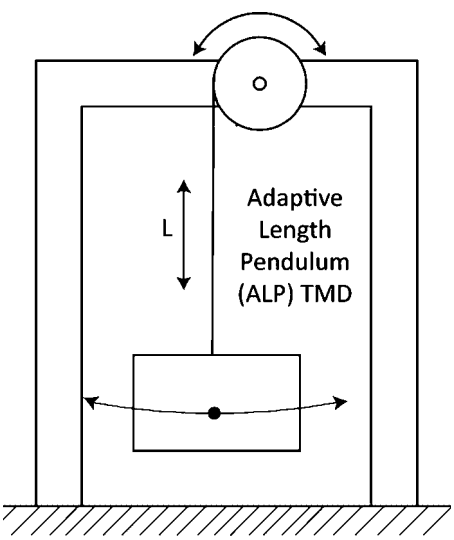

Figure 32. ALP STMD or APTMD.

DOI: 10.1002/stc

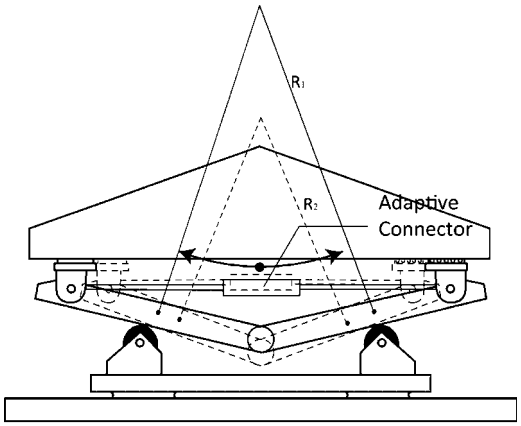

Figure 33. Adaptive radius APTMD or STMD.

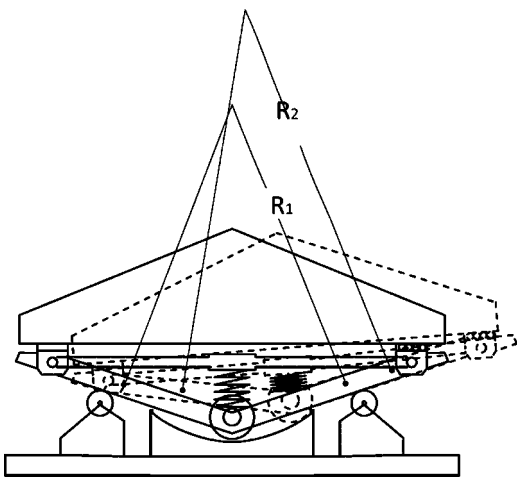

Figure 34. Adaptive radius based APTMD.

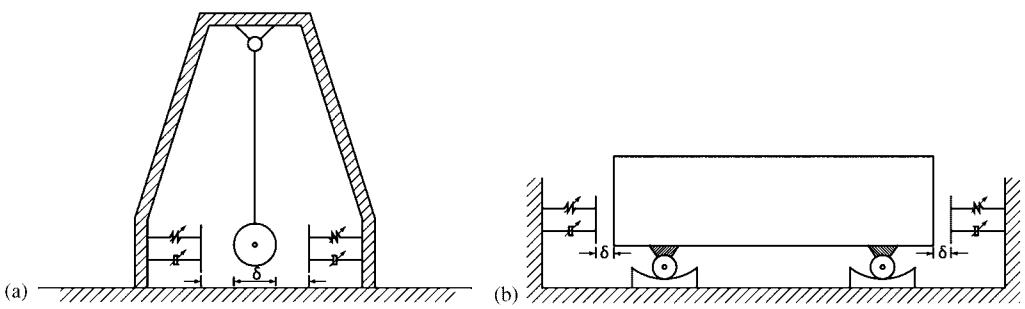

Figure 35. Displacement based APTMD.

DOI: 10.1002/stc

possible adaptive passive TMD is shown in 35(b), wherein the concave surfaces on which the support rollers move can be shaped/tuned and in addition once the mass contacts the ASD device further adaptation is possible (by adjustment of the valves in the ASD device).

8. PRACTICAL STMD AND APTMD CONCEPTS AND THEIR IMPLEMENTATION

In this section we present implementation of STMD's and APTMD's in USA, Japan, and China, either based on the concepts and ideas presented in this paper or developed independently by others, but similar in nature.

8.1. Citicorp building TMD: STMD

The Citicorp center building in New York city [18] has a passive TMD with an active control component, which is auxiliary in nature. The author was aware of the TMD [17], but was not aware of the specifics of its implementation. One of the anonymous reviewers of this paper alerted the author regarding the paper by Peterson [18], for which the author is grateful to the reviewer.

The details of the implementation in Citicorp building presented by Peterson [18] are that the building has a first mode frequency of 6.9 s in the North–South direction and 7.2 s in the East–West direction, with nearly 1% damping in each direction. The 820 kip TMD is supported on low friction (0.003 coefficient of friction) hydraulic pressure balanced bearings. The TMD is attached to nitrogen springs of stiffness 3.2 kips/in, shown in Figure 36, in both N-S and E-W directions. In addition, the mass is also attached to servo-controlled hydraulic actuators (both in the N-S and E-W directions) that are used to adjust the stiffness or frequency and damping of the TMD.

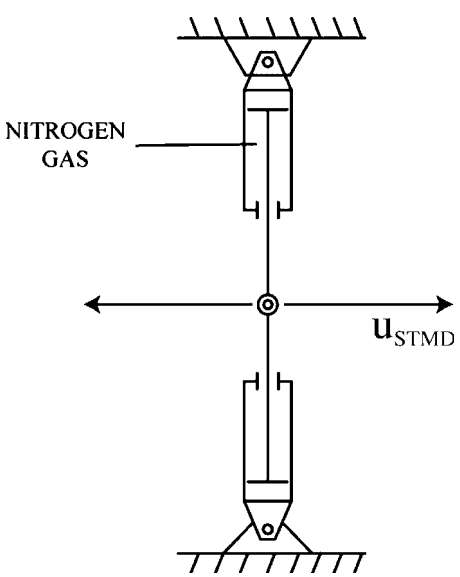

Figure 36. Citi Corp TMD nitrogen springs.

DOI: 10.1002/stc

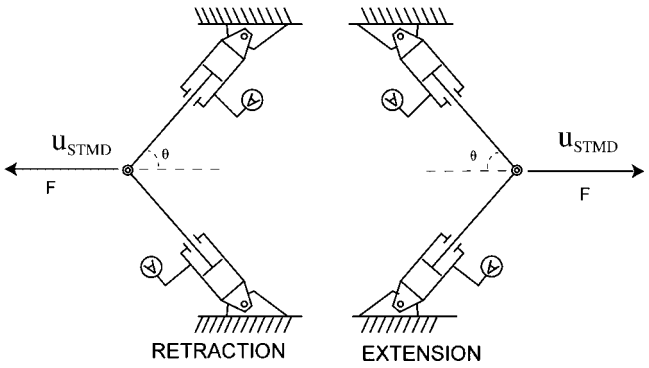

Figure 37. Citi Corp TMD nitrogen springs.

The nitrogen gas spring consists of two opposed pneumatically pre-charged cylinders that are trunnion mounted with piston rods connected as shown in Figure 36; when the cylinders deflect perpendicular to their axis, as shown in Figure 37, the inherent nonlinearity of the adiabatic gas compression in a closed vessel is almost exactly compensated by the geometric nonlinearity due to the angle θ. This leads to essentially a linear pneumatic spring. A further advantage of the gas spring is that only simple adjustment of the precharge pressure in the nitrogen cylinder is necessary to vary the spring rate, thus, the spring stiffness.

The primary restoring force/stiffness to tune the TMD is provided by the pneumatic nitrogen springs and only finer adjustments are made using the active control. The active hydraulic actuators are also used to overcome the friction in bearings (very nominal because of low friction) that support the TMD. The actuators play an auxiliary role; hence, the system is primarily a passive TMD with an auxiliary active component. As implemented this is an STMD; since, the active control part is used primarily to fine tune the stiffness and damping of the TMD as in an STMD, the rest of the work is done by the passive TMD. This strategy is used to keep the active part auxiliary and keep the associated power requirements to a minimum. Recall this was described—in the introduction—as one of the primary advantages of the STMD when compared to an active TMD. Also, to save energy, triggers based on acceleration threshold (3 mg for two cycles) are used to turn the active part on and then after 30 min to return it to standby mode, if the acceleration does not exceed 0.75 mg.

It is worth noting that a possible APTMD is based on passive version of SAIVS with nitrogen gas springs replacing the mechanical springs, and a screw jack replacing the linear electromechanical actuator. This would allow easy adjustment of stiffness to tune the TMD, when necessary, as in Citicorp building TMD.

8.2. Tokyo towers adaptive radius TMD: APTMD

Another idea similar to the pendulum is a TMD with a radius of oscillation. This is precisely what has been accomplished in developing the V-shaped Hybrid Mass Damper (HMD) by Ishikawajima Heavy industries, because the radius L is adjusted by changing the angle of the V-shaped rail. Tokyo Park Tower is equipped with three HMD's of this type (Koike *et al.* [51]). The change in V-shaped rail radius is accomplished using motors and servo-controllers, not in real time, but offline, making this an APTMD (Figure 38).

DOI: 10.1002/stc

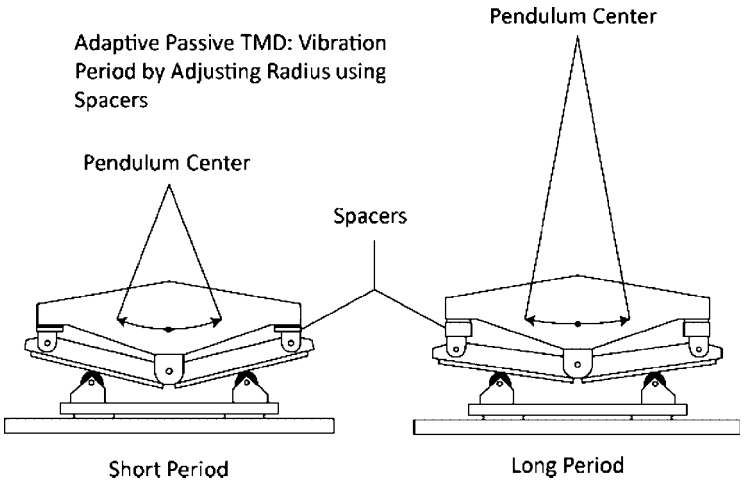

Figure 38. Adaptive radius APTMD—Tokyo Park Tower.

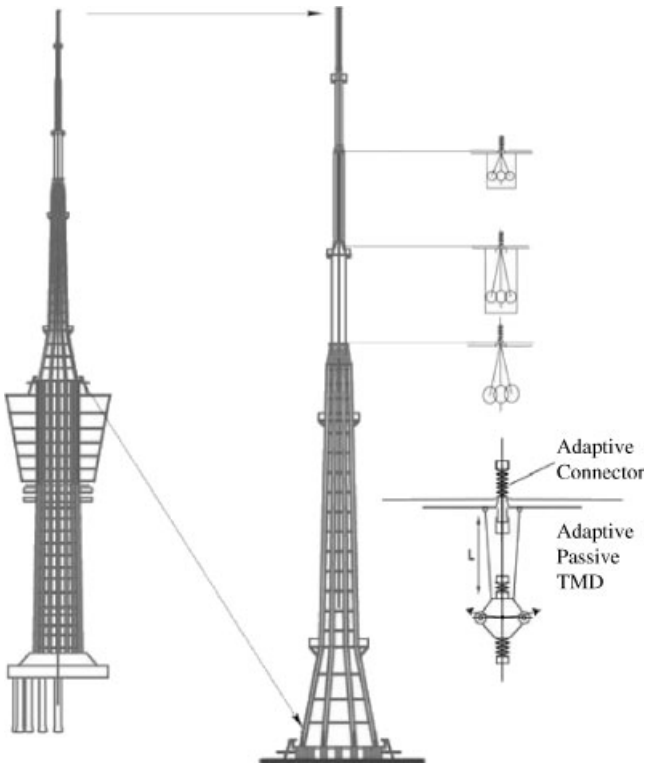

Figure 39. APTMD: ShenZhen WuTong TV Tower.

DOI: 10.1002/stc

8.3. ShenZhen WuTong TV tower and Guangzhou New TV tower: APTMD

The ShenZhen WuTong mountain TV tower, in China, near Hong Kong, with a total height of 198 m was completed recently. The TV tower has a series of adaptive passive TMD or ALP in which the length of the pendulum is mechanically adapted [52], as shown in Figure 39 (Teng and Ou [53]). The adaptation occurs passively and no servo-control is used in this application, making it an APTMD. The Guangzhou New TV tower, Guangzhou, China, with a total height of 610 m was completed recently. It consists of two APTMD's in the TV tower [54, 55].

9. CONCLUSIONS

The effectiveness of the developed time-frequency algorithms for system identification and control the response of MDOF systems with STMD has been demonstrated by simulated and experimental results. The EMD/HT and STFT algorithms applied to MDOF with STMD produce real time retuning to reduce the response under harmonic, sine-sweep and white-noise (stationary) and earthquake (non-stationary) excitations. It is found that the TMD loses its effectiveness even with just 5% mistuning, where as, STMD retunes and reduces the response effectively. The algorithms presented in this paper demonstrate the powerful capabilities of time-frequency methods for structural control and system identification.

The new ALP STMD and the adaptive passive APTMD proposed in this study have a great deal of promise for practical implementation. APTMD is a TMD in which the frequency is adjusted by either changing the length of pendulum or by changing the radius of surface on which the mass oscillates; but without associated sensing and computer feedback needed in a STMD.

Additionally, a number of practical STMD and APTMD concepts and their implementation in USA, Japan, China has been presented. STMD and APTMD offer a number of new possibilities for response control of flexible structures, such as tall buildings and long span bridges, under wind and earthquake loading.

ACKNOWLEDGEMENTS

The author thanks Professors Fujino and Nishitani for inviting this contribution for the Kobori special issue of the Journal of Structural Control and Health Monitoring. The author acknowledges the assistance of Dr N. Varadarajan in preparing this paper. The author gratefully acknowledges the support of National Science Foundation grants, NSF CMMI 0830391 for study and development of new Practical Adaptive Passive Stiffness and Damping Systems including APTMD and ALP TMD. In addition, author gratefully acknowledges the support of NSF CMS CAREER grant 9996290 for study of variable stiffness systems, smart tuned mass dampers, and time-frequency algorithms for identification and control.

REFERENCES

1. Nishitani A. Obituary for Professor Takuji Kobori (1920–2007): great pioneer in structural dynamics and control. *Structural Control and Health Monitoring* 2008; **15**(2):117–119.
2. Kobori T. Towards a common goal via different road. *Structural Control and Health Monitoring* 2006; **13**(1):7–9.
3. Kobori T, Takahashi M, Nasu T, Niwa N, Ogasawara K. Seismic response controlled structure with active variable stiffness system. *Earthquake Engineering and Structural Dynamics* 1993; **22**(11):925–941.

DOI: 10.1002/stc

4. Yamada K, Kobori T. Control algorithm for estimating future responses of active variable stiffness structure. *Earthquake Engineering and Structural Dynamics* 1995; **24**(8):1085–1099.
5. Chang JCH, Soong TT. Structural control using active tuned mass dampers. *Journal of Engineering Mechanics* (ASCE) 1980; **6**(106):1091–1098.
6. Ikeda Y, Sasaki K, Sakamoto M, Kobori T. Active mass driver system as the first application of active structural control. *Earthquake Engineering and Structural Dynamics* 2001; **30**(11):1575–1595.
7. Reinhorn A, Soong TT, Riley MA, Lin RC, Aizawa S, Higashino M. Full sale implementation of active control. II: installation and performance. *Journal of Structural Engineering* (ASCE) 1993; **6**(119):1935–1960.
8. Kurata N, Kobori T, Takahashi M, Niw N, Midorikawa H. Actual seismic response controlled building with semi-active damper system. *Earthquake Engineering and Structural Dynamics* 1999; **28**:1427–1447.
9. Spencer B, Nagarajaiah S. State of the art of structural control. *Journal of Structural Engineering* (ASCE) 2003; **129**(7):845–856.
10. Chu SY, Soong TT, Reinhorn AM. *Active, Hybrid, Semi-Active Structural Control—A Design and Implementation Handbook*. Wiley: New York, 2005. ISBN-13 978-0-470-01352-6.
11. Yang JN, Kim J, Agrawal AK. Resetting semiactive stiffness damper for seismic response control. *Journal of Structural Engineering* (ASCE) 2000; **126**(12):1427–1433.
12. Yang JN, Bobrow J, Jabbari F, Leavitt J, Cheng CP, Lin PY. Full-scale experimental verification of resetable semi-active stiffness dampers. *Earthquake Engineering and Structural Dynamics* 2007; **36**(9):1255–1273.
13. Nagarajaiah S. Structural vibration damper with continuously variable stiffness. US Patent No. 6098969, 2000.
14. Nagarajaiah S, Mate D. Semi-active control of continuously variable stiffness system. *Proceedings of the Second World Conference on Structural Control*, vol. 1, Kyoto, Japan 1998; 397–405.
15. Den Hartog JP. *Mechanical Vibrations* (4th edn). McGraw-Hill: New York, 1956.
16. Ormondroyd J, Den Hartog JP. The theory of the dynamic vibration absorber. *Transactions of ASME* 1928; APM-50-7, 9-22.
17. McNamara RJ. Tuned mass dampers for buildings. *Journal of the Structural Division* (ASCE) 1977; **103**(9): 1785–1798.
18. Peterson NP. Design of large scale tuned mass dampers. In *Structural Control*, Leipholz HHE (ed.). IUTAM, North-Holland Publishing Company, SM Publications: Amsterdam, The Netherlands, 1980.
19. Fujino Y, Sun L, Pacheco BM, Chaiseri P. Tuned liquid damper (TLD) for suppressing horizontal motion of structures. *Journal of Engineering Mechanics* (ASCE) 1922; **118**:(10):2017–2030.
20. Abe M, Fujino Y. Dynamic characterization of multiple tuned mass dampers and some design formulas. *Earthquake Engineering and Structural Dynamics* 1994; **23**:813–835.
21. Fujino Y, Sun LM. Vibration control by multiple tuned liquid dampers (MTLDs). *Journal of Structural Engineering* (ASCE) 1993; **119**(12):3482–3502.
22. Igusa T, Xu K. Vibration control using multiple tuned mass dampers. *Journal of Sound and Vibration* 1994; **175**(4): 491–503.
23. Jangid RS. Optimal multiple tuned mass dampers for base-excited undamped system. *Earthquake Engineering and Structural Dynamics* 1999; **28**:1041–1049.
24. Kareem A, Kline S. Performance of multiple mass dampers under random loading. *Journal of Structural Engineering* (ASCE) 1993; **2**(121):348–361.
25. Yamaguchi H, Harnpornchai N. Fundamental characteristics of multiple tuned mass dampers for suppressing harmonically forced oscillations. *Earthquake Engineering and Structural Dynamics* 1993; **22**(1):51–62.
26. Abe M, Igusa T. Semi-active dynamic vibration absorbers for controlling transient response. *Journal of Sound and Vibration* 1996; **5**(198):547–569.
27. Bonellol P, Brennan MJ, Elliott SJ. Vibration control using an adaptive tuned vibration absorber with a variable curvature stiffness element. *Smart Materials and Structures* 2005; **14**:1055–1065.
28. Franchek MA, Ryan MW, Bernhard RJ. Adaptive passive vibration control. *Journal of Sound and Vibration* 1995; **189**(5):565–585.
29. Hrovat D, Barak P, Rabins M. Semiactive versus passive or active tuned mass dampers for structural control. *Journal of Engineering Mechanics* (ASCE) 1982; **3**(109):691–705.
30. Lai JS, Wang KW. Parametric control of structural vibrations via adaptable stiffness dynamic absorbers. *Journal of Vibrations and Acoustics* (ASME) 1996; **118**(1):41–47.
31. Nagarajaiah S, Varadarajan N. Semi-active control of wind excited building with variable stiffness TMD using short time Fourier transform. *Journal of Engineering Structures* 2005; **27**:431–441.
32. Nagarajaiah S, Sonmez E. Structures of semiactive variable stiffness multiple tuned mass dampers under harmonic forces. *Journal of Structural Engineering* (ASCE) 2007; **133**(1):67–77.
33. Sun JQ, Jolly MR, Norris MA. Passive, adaptive, and active tuned vibration absorbers: a survey. *Journal of Mechanical Design* 1995; **111**(B):234–242. 50th Anniversary Issue of ASME Journal of Vibration and Acoustics.
34. Yalla SK, Kareem A, Cantor JC. Semi-active tuned liquid dampers for vibration control of structures. *Engineering Structures* 2001; **23**:1469–1479.

DOI: 10.1002/stc

35. Varadarajan N, Nagarajaiah S. Wind response control of building with variable stiffness tuned mass damper using EMD/HT. *Journal of Engineering Mechanics* (ASCE) 2004; **130**(4):451–458.
36. Nagarajaiah S, Varadarajan N. Novel semi-active variable stiffness tuned mass damper with real time tuning capability. *Proceedings of 13 Engineering Mechanics Conference* (ASCE), UT-Austin, CD ROM, 2000.
37. Nagarajaiah S, Varadarajan N. Semi-active control of smart tuned mass damper using empirical mode decomposition and hilbert transform algorithm. *Proceedings of ICOSSAR 2001*, Newport Beach, CA, June, CD ROM, 2001.
38. Basu B, Nagarajaiah S. A wavelet-based time-varying adaptive LQR algorithm for structural control. *Journal of Engineering Structures* 2008; **30**(9):2470–2477.
39. Basu B, Nagarajaiah S, Chakraborty A. Online identification of linear time-varying stiffness of structural systems by wavelet analysis. *International Journal of Structural Health Monitoring* 2008; **7**(1):21–36.
40. Cohen L. *Time-Frequency Analysis* (1st edn). Prentice-Hall: New Jersey, 1995.
41. Huang EN, Shen Z, Long RS, Wu CM, Shih HH, Zheng Q, Yen N, Tung CC, Liu HH. The empirical mode decomposition and the hilbert spectrum for nonlinear and non-stationary time series analysis. *Procedings of the Royal Society of London* 1998; **454**:903–995.
42. Rilling G, Flandrin P, Goncalves P. On empirical mode decomposition and its algorithms. *IEEE-EURASIP Workshop on Nonlinear Signal and Image Processing* 2003. NSIP-03, Grado I.
43. Nagarajaiah S, Vardarajan N, Sahasrabudhe S. Variable stiffness and instantaneous frequency. *Proceedings of Structures Congress* (ASCE) 1999; **1**:858–861.
44. Thrane N. The Hilbert transform. BV0015, *Bruel Kjaer Technical Review* 1984; **3**:3–15 (ISSN 007-2621).
45. Agneni A, Balis-Cerma L. Damping measurements from truncated signals via the Hilbert transform. *Mechanical Systems and Signal Processing* 1989; **3**(1):1–3.
46. Yang JN, Lei Y, Pan S, Huang N. System identification of linear structures based on Hilbert-Haung spectral analysis part I: normal modes. *Earthquake Engineering and Structural Dyanmics* 2003; **32**:1443–1467.
47. Yang JN, Lei Y, Lin S, Huang N. Hilbert-Haung based apporach for structural damage detection. *Journal of Engineering Mechanics* 2004; **130**(1):85–95.
48. Nagarajaiah S, Sahasrabudhe S. Seismic response control of smart sliding isolated buildings using variable stiffness systems: experimental and numerical study. *Earthquake Engineering and Structural Dynamics* 2006; **35**(2):177–197.
49. Narasimhan S, Nagarajaiah S. STFT algorithm for semiactive control of base isolated buildings with variable stiffness isolation systems subjected to near fault earthquakes. *Engineering Structures* 2005; **27**:514–523.
50. Dyck J, Nagarajaiah S, Taylor D. Variation of supplemental stiffness and damping using adjustable fluid spring and damper. *Proceedings of the 8th U.S. National Conference on Earthquake Engineering*, EERI, CDROM, 2006.
51. Koike Y, Tanida K. Application of V-shaped hybrid mass damper to high rise buildings and verification of the damper performance. *Proceedings of the Structural Engineers World Congress*, San Francisco 1998, T198-4 (CD-ROM).
52. Yan AZ, Teng J, Lu ZX. Analysis for seismic response of Wutong TV-Tower with variable stiffness tuned mass dampers. *4th International Conference on Earthquake Engineering*, *Taipei*, *Taiwan* 2006. Paper No. 186.
53. Teng J, Ou J. The New Shenzhen Wutong Mountain TV Tower. Personal Communications. 2008.
54. Ni YQ, Xia Y, Liao WY, Ko JM. Technology innovation in developing the structural health monitoring system for Guangzhou New TV tower. *Structural Control and Health Monitoring* 2009; **16**(1):73–98.
55. Ni YQ. Guangzhou New TV Tower. Personal Communication. 2009.

DOI: 10.1002/stc